Characteristics of debris avalanche deposits inferred from source volume estimate and hummock morphology around Mt Erciyes, central Turkey

Yuichi S. Hayakawa[1], Hidetsugu Yoshida[2], Hiroyuki Obanawa[3], Ryutaro Naruhashi[4], Koji Okumura[5], Masumi Zaiki[6], Ryoichi Kontani[7]

[1]Center for Spatial Information Science, The University of Tokyo, Kashiwa, 277-8568, Japan
[2]School of Arts and Letters, Meiji University, Tokyo, 101-8301, Japan
[3]VisionTech Inc., Tsukuba, 305-0045, Japan
[4]Earthquake Research Institute, The University of Tokyo, Tokyo, 113-0032, Japan
[5]Department of Geography, Graduate School of Letters, Hiroshima University, Hiroshima, 739-852, Japan
[6]Department of Economics and Business, Faculty of Economics, Seikei University, Tokyo, 180-8633, Japan
[7]Department of Contemporary Sociological Studies, Faculty of Literature, Notre Dame Seishin University, Okayama, 700-8516, Japan

Correspondence to: Yuichi S. Hayakawa (hayakawa@csis.u-tokyo.ac.jp)

Abstract. Debris avalanche caused by volcano sector collapse often forms characteristic depositional landforms such as hummocks. Sedimentological and geomorphological analyses of debris avalanche deposits (DAD) are crucial to clarify the size, mechanisms, and emplacement of debris avalanches. We describe the morphology of hummocks on the northeastern flank of Mt. Erciyes in Kayseri, central Turkey, likely formed in the late Pleistocene. Using a remotely piloted aircraft system (RPAS) and the structure-from-motion multi-view stereo photogrammetry (SfM), we obtained high-definition digital elevation model (DEM) and orthorectified ~~image~~ of the hummocks~~, whose~~ geometric features ~~are investigated~~. We estimated the source volume of the DAD by reconstructing the ~~original shape of the mountain body~~ using a satellite-based DEM. ~~For this, we~~ examined the topographic cross sections based on the slopes around the scar regarded as remnant topography ~~preserved since the sector collapse~~. Spatial distribution of hummocks is anomalously concentrated at a certain distance from the source, unlike those that follow the distance-size relationship. The high-definition land surface data by RPAS and SfM revealed that many of the hummocks are aligned toward the flow direction of the debris avalanche, suggesting that the extensional regime of the debris avalanche was dominant. However, some displaced hummocks were also found, indicating that the compressional regime of the flow contributed to the formation of hummocks. These indicate that the flow and emplacement of the avalanche were constrained by the topography. The existing caldera wall forced the initial eastward flow to move northward, and the northside ~~of the~~ wall ~~barriered~~ the flow ~~to become once compressional regime, but~~ the narrow and steepened outlet valley ~~forced the flow to become extentional again~~. Also, the estimated volume of 12–15 × 10^8 m^3 gives a mean thickness of 60–75 m, which is much deeper than the reported cases of other DADs. This suggests that the debris avalanche must have ~~flown down far~~ downstream and beyond the current DAD extent. Assessments of the DAD incorporating the topographic constraints can provide further insights into the risk and mitigation of potential disasters in the study area.

1 Introduction

Catastrophic sector collapses are often observed in volcanoes when they become structurally and gravitationally unstable ~~and~~ are triggered by earthquakes, magma intrusion, or phreatic eruptions (Siebert, 1984, 1992; Ui et al., 2000). This phenomenon is hazardous because of a large amount of mass movement involved that appears as a debris avalanche moving at high speed (Ui, 1975; Vallance et al., 1995; Glicken, 1996; Vallance and Scott, 1997; Yoshida and Sugai, 2006). Furthermore, sector collapse can repeatedly occur on the same volcano after regrowing an unstable flank (Tibaldi and Vezzoli, 2004; Zernack et

al., 2009). Such the recurrence of sector collapse is often expected not only in one direction but a different, or multiple directions (Lagmay et al., 2000; Yoshida and Sugai, 2007; Paguican et al., 2012, 2014). However, since the recurrence interval is not constant and the stationary period can last for more than 10^3 to 10^4 years (Moriya, 1988), the areas around an unstable volcano can be highly urbanized without the consideration of the risk of the sector collapse. In particular, the downstream area of debris avalanche deposits is often flat enough to be urbanized or cultivated. In such urbanized areas, detailed information of the past debris avalanche including its timing, size, and kinematics is crucial for the future hazard assessment.

Debris avalanche caused by a volcanic sector collapse forms characteristic depositional landforms called hummocks, composed of large block facies within a matrix (Siebert, 1984; Ui et al., 1986, 2000; Orton, 1996). Within the domain of debris avalanche deposits (DAD), hummocks often have clear boundaries and are readily identifiable, thus providing a chance to carry out the robust size and shape analysis (Mizuno, 1958; Hashimoto et al., 1979). Such the morphology of hummocks, located on the surface of DADs, can be used to estimate the characteristics of the debris avalanche, i.e., the kinematics of the sliding mass of the sector collapse (Dufresne and Davies, 2009; Koarai et al., 2008; Yoshida and Sugai, 2010; Yoshida, 2012, 2013, 2014; Yoshida et al., 2012). Although sedimentological investigations of the internal structures of DADs often provide insights into the transport mechanisms (e.g., Glicken, 1996; Bernard et al., 2008; Shea et al., 2008), geomorphological or geometrical analyses of the surficial morphology of DADs including hummocks can also provide estimations on the size and processes of the debris avalanche. In particular, because the sedimentary structure is mutually related to the hummock distribution and shape, the distribution and morphology of hummocks formed in DADs provide an opportunity to examine the volumetric and kinematic characteristics of the debris avalanche (Dufrense and Davies, 2009; Yoshida and Sugai, 2010; Yoshida et al., 2012). During the sliding of a sector collapse, the fractured mass of the original volcanic edifice forms collapse structures along with the alternate regimes of extension and compression (Paguican et al., 2012, 2014). This often results in the alternate extensional/compressional structures of DADs along the avalanche course, while the compressional regime may result in the denser distribution of hummocks particularly around the flow front (Yoshida et al., 2012).

Hummocks are often in the order of tens to hundreds of meters in size, so aerial photographs are often used for their identification and morphological analysis (Glicken, 1996; Yoshida, 2012, 2013, 2014; Yoshida and Sugai, 2010; Yoshida et al., 2012). Digital elevation models (DEM) by airborne laser scanning (ALS) within 1–5 m resolution can also be used for such analysis (e.g., Hayakawa et al., in press), but such high-definition data including paired aerial photographs and ALS-DEMs are often unavailable in many areas. High-definition satellite remote sensing imagery and DEMs can also be used for the analysis of hummocks, but the acquisition cost is often high and may not be readily obtained in many cases. Due to availability, details of many known DADs remain unexamined.

Recent developments in the remotely-piloted aerial system (RPAS), as well as that in the structure-from-motion multi-view (SfM-MVS) photogrammetry, have enabled on-site, cost-efficient acquisition of high-definition topographic and imagery data (e.g., Westoby et al., 2012; Fonstad et al., 2013; Obanawa et al., 2014; Hayakawa et al., 2016). Such detailed earth surface data are useful for detailed topographic analysis, including topographic feature extraction and landform classifications, for areas of approximately 0.1–10 km^2 that cannot be achieved by low-resolution satellite imagery (e.g., Koarai et al., 2008). Moreover, although ordinary aerial photographs taken by manned aircraft have often been utilized to investigate topographic features of DADs in such a small- to medium-sized area (Siebert, 1984; Glicken, 1996; Yoshida and Sugai, 2007, 2012), high-quality stereo-paired aerial photographs are often unavailable in many areas over the world. Without the availability of ordinary aerial photographs, RPAS-derived land surface data (topography and imagery) are therefore useful enough even if not fully taking the advantage of its highest resolution. Furthermore, the higher resolution data acquired by RPAS should serve as a potential archive for future studies, because the rapid increase in the use of RPAS will enable further data collection of such high-definition data in many areas.

Using the combined RPAS- and satellite-derived topographic data, we analyze the morphology of hummocks and DAD on the northeast flank of Mt. Erciyes, previously described by Şen et al. (2003). We use RPAS for the acquisition and analysis of detailed, high-definition morphological data for the hummocks formed on the DAD, where ordinary stereo-paired aerial photographs nor ALS-derived topographic data are unavailable. The high-definition topographic data are crucial for the identification and analysis of 10- to 100-m scale hummocks. We also utilize topographic data at 10 m resolution from satellite SAR imagery for the analysis of the surrounding areas. The volume of the DAD crucial for describing the sector collapse, which is hard to know from the extent and depth of the deposits, is obtained by reconstructing the original topography of the source area.

2 Study area

Mt. Erciyes, located in the south of Kayseri City in central Turkey (Fig. 1), is the highest stratovolcano in this region with an elevation of 3917 m at its summit. The current ~~mountain body of the volcano~~ has been formed after the pre-Erciyes volcanic activities terminated about 3 Ma with an extensive ignimbrite eruption (Innocenti et al., 1975; Şen et al., 2003). The stratigraphy of Mt. Erciyes ~~comprise~~ basaltic, ~~andesite~~, and dacitic lava flows in ca. 2.5–0.2 Ma, followed by pumice and pyroclastic flow deposits (Şen et al., 2003).

The youngest deposit is the DAD, emplaced after 83 ka (Şen et al., 2003). Moraines that formed in the last glacial maximum (21.3 ka) are also present in the valley along the avalanche flow (Üçker Valley, A in Fig. 1) (Sarıkaya et al., 2009). This gives an approximate age of the sector collapse of between 20–80 ka.

The DAD is observed within 2–9 km downstream along a fluvial valley from the mountain top, covering an area of ~14 km^2 (Şen et al., 2003) (B and northern part of C in Fig. 1). The downstream extent, however, is hard to identify due to limited exposure, and erosion and remobilization of DAD after emplacement, particularly in the fluvial valley. Nevertheless, we found several outcrops of the DAD along a newly constructed highway~~, whose~~ locations are shown as stars in Fig. 1. The farthest outcrop is ~~found to be~~ 16 km away from the summit of Mt. Erciyes. Moreover, ~~as noted later,~~ hummocks ~~of the DAD~~ appear ~~in~~ 11–13 km downstream from the summit. These indicate that the potential extent of the DAD is ~~much more~~ downstream over the area mapped by Şen et al. (2003), with an area ~~of no less~~ than 20 km^2.

Based on the collapse scar, the debris avalanche was supposed to be flowing to the east (A in Fig. 1, Fig. 2a). The flow then turned to the north due to confinement by pre-existing caldera walls. Unfortunately, we could not find any outcrops in the field including abutting deposits on the footslopes of caldera wall. However, the present lake, located in the south of the bend of the DAD and now serves as a reservoir, is possibly a remnant of a dammed lake ~~(D in Fig. 1). At least,~~ it is clear that the debris avalanche flow did not largely turn to the south, but followed northward along the pre-existed caldera wall.

Hummocks, characteristic mound-shaped topographic features of DADs, are densely ~~and only found~~ in an approximately 2 km^2 area around 11–13 km (along-valley distance) from the summit of Mt. Erciyes. Our topographic measurements, therefore, focus on this domain. As noted, this domain of hummocks is out of the range of the DAD area previously reported (B in Fig. 1; Şen et al., 2003), but the potential extent of the DAD likely covers this domain ~~to the~~ farther downstream. As far as we investigate, no hummock is observed in other areas of the DAD along the valley. Mound-shaped features on the eastern side of the DAD (C in Fig. 1) are basaltic or ~~andesite~~ lava domes~~, as confirmed in the field.~~

~~A~~ left-lateral strike slip ~~fault, named as the~~ Erciyes Fault as a member of the Ecemiş Fault ~~group of the East Anatolian Fault zone,~~ is mapped to potentially cut across the Mt. Erciyes along the north-northeast direction (Emre et al., 2011). The age and history of the fault activity, however, are not well known.

The climate in the area is warm and dry, with an annual precipitation of ~400 mm, resulting in scarce vegetation cover. Climatic fluctuations including relatively wet periods in the late Pleistocene to Holocene has been dry enough not to grow dense vegetation since the last interglacial (Kuzucuoglu et al., 1999; Bayer Altin et al., 2015; Pickarski et al., 2015). Hence,

the slope processes have not been so active to significantly modify the topography~~, particularly in the dry periods~~. The original topography of the debris avalanche, as well as the landforms surrounding the sector collapse, is therefore supposed to be well preserved, except for areas around valley bottoms where fluvial or glacial modifications have been active and volcanic alluvial fans are well developed.

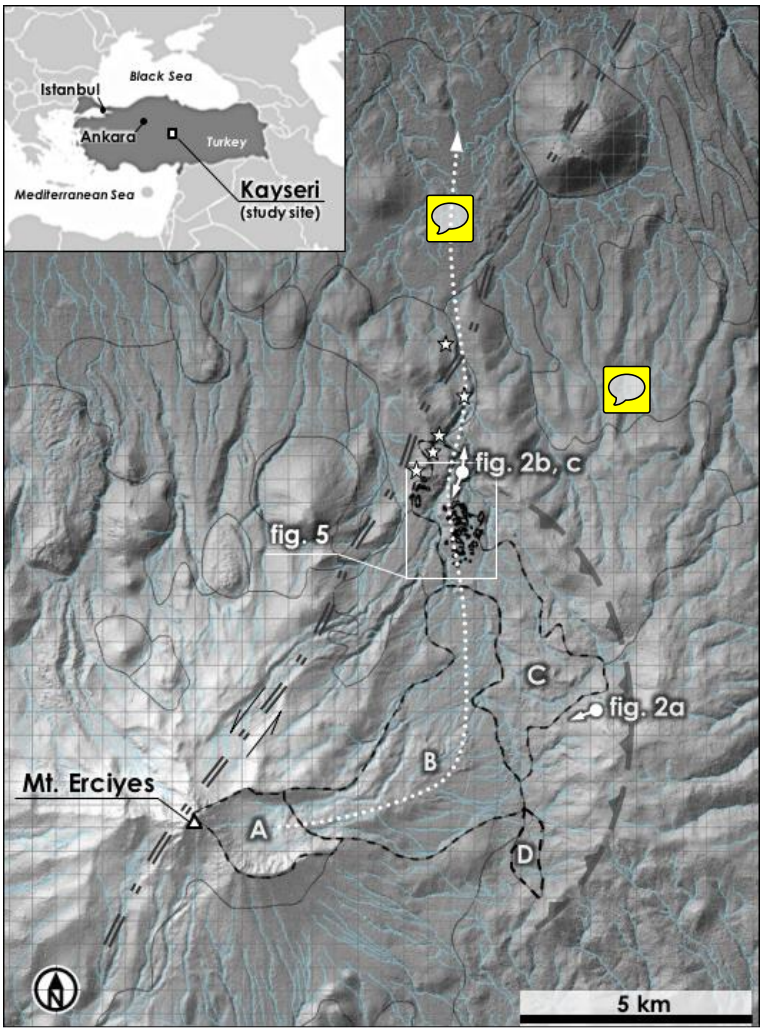

Figure 1: Map of the study area. Thin solid gray lines indicate the boundaries of lithological units reported by Şen et al. (2003). Units surrounded by dashed, solid black lines with alphabets show the sector collapse source (A), DAD (B), andesite lava domes (C), and a lake (D), respectively. Note that the northern half of the lava domes (C) previously mapped by Şen et al. (2003) is in fact the DAD. Stars locate outcrops of the DAD found in this study, and the estimated course of the debris avalanche in this study is shown as dotted white arrow. Black solid polygons within the extent of Figure 6 are the hummocks examined. Dashed curving gray line with triangles indicates the remnant of caldera walls before the formation of modern Mt. Erciyes. Dashed double line shows the approximate path of the Erciyes Fault mapped by Emre et al. (2011).

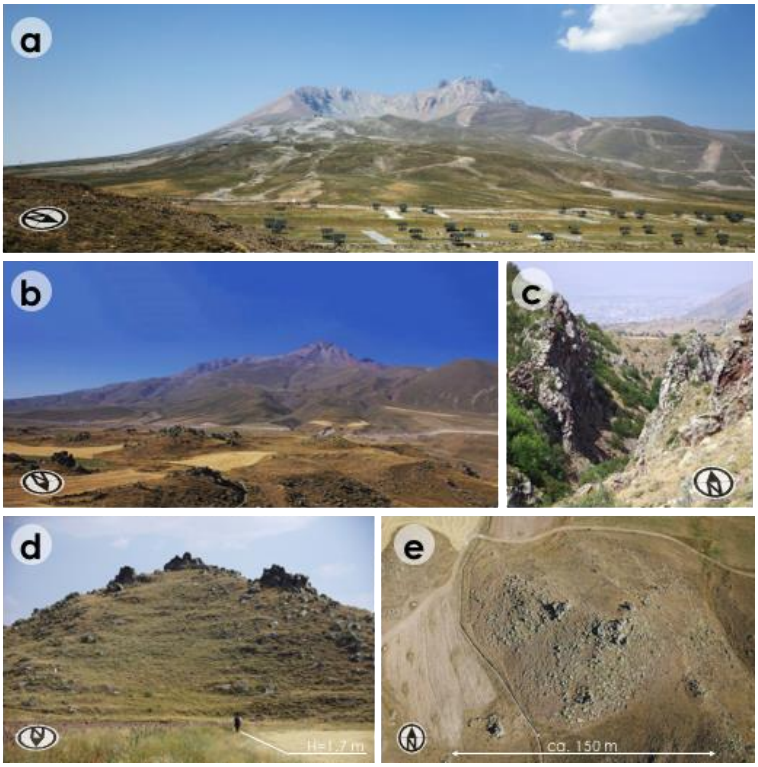

Figure 2: Pictures of the study area. Locations of these photos are shown in Figure 1. (a) Collapse scar of Mt. Erciyes, photo taken westward. On the foreground is where the avalanche changed direction from east to north. The relative height of the mountain body is 1800 m (~2100 m a.s.l. on the foreground DAD surface and 3917 m a.s.l. at summit). (b) Mt. Erciyes and the 10- to 100-m sized hummocks on the foreground, photo taken southward. (c) Downstream view of deeply-incised gorge past the hummock-dominated area, photo taken northward. The incision depth is ~40 to 60 m. (d) Ground-based view of a hummock, ~30 m high, photo taken southward. (e) Aerial view of hummock in d with a diameter of ~150 m (photo without distortion correction).

3 Methods

3.1 RPAS-based SfM-MVS photogrammetry and hummock mapping

To measure the detailed surface morphology of the DAD, we apply the SfM-MVS photogrammetry using low-altitude aerial photographs taken by an RPAS. (Fig. 3) The RPAS~~, including~~ a small unmanned aerial vehicle (UAV) equipped with a digital camera~~, enables to obtain~~ low-altitude aerial photographs in the field. The image data obtained are used to capture ~~the data of~~ earth surface condition and morphology ~~in a~~ relatively broad ~~area~~, typically for 0.1–10 km^2. We used two UAVs for the measurement: DJI Phantom 2 on which a ~~digital camera of~~ Nikon Coolpix A (sensor resolution: 4928 × 3264 pixels, 35-mm equivalent focal length: 28 mm) or RICOH GR (sensor resolution: 4928 × 3264 pixels, 35-mm equivalent focal length: 28 mm) is mounted, and DJI Phantom 3 Professional with a built-in stabilized camera FC300X (sensor resolution: 4000 × 3000 pixels, 35-mm equivalent focal length: 20 mm).

~~We carried out the flights of the~~ UAVs from several locations in and around the ~~area with hummocks~~. The UAVs were manually operated, and ~~the~~ flight courses were ~~successively~~ set to cover the area of interest sufficiently. During ~~the~~ flights, the camera shutter ~~is set to work~~ automatically ~~at an interval of 2 seconds~~. A flight of ~10 to 20 minutes takes 300–600 photographs.

Geographical coordinates of several ground control points (GCP) were obtained, using a post-processed kinematic global navigation satellite system (GNSS) receiver. Trimble GeoExplorer 6000XH was used as the GNSS rover, with log data corrected using the fixed GNSS base station of the International GNSS Service (IGS) network. The GCPs ~~were placed~~ in the main target area around the hummocks. Characteristic objects that are readily identifiable in the aerial photographs

were selected as ~~such~~ GCPs~~, including~~ road intersections, flat stone surfaces on bridges, and large ~~rock blocks with flat tops~~. The projection of the geographical coordinates is set to UTM zone 36N on WGS 84 (EPSG:32636).

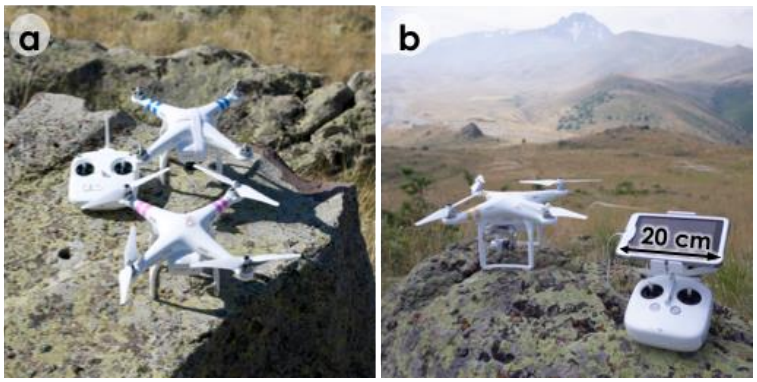

Figure 3: RPAS used in this study. (a) DJI Phantom 2. External digital cameras of Nikon Coolpix A and RICOH GR are attached. (b) DJI Phantom 3 Professional with a built-in digital camera.

~~Using hundreds of aerial photographs taken by the RPAS, we~~ ~~carry~~ out ~~the~~ SfM-MVS photogrammetry~~. The photogrammetric software used was~~ PhotoScan Professional Edition by Agisoft LLC. From multiple photographs, ~~the~~ SfM process provides three-dimensional positions of the stereo-paired photographs, in which the same features are identified among the paired photographs as tie points. Although geographical coordinates of the camera locations can be known from the GNSS records in the built-in camera of the UAV devices, the positional accuracies of the single-source GNSS receiver of the UAVs are low, being on the order of meters. The GCPs whose coordinates are obtained by the post-processed GNSS receiver are therefore placed in the image data to ~~achieve better~~ positional accuracies. The tie point cloud is adjusted to fit the GCPs, and the points with large reprojection errors (≥1.0 pixels) are removed. By the MVS-photogrammetric process, denser three-dimensional points are ~~then~~ further obtained from the aligned and paired images. Based on the resultant point density and ground resolution of the images, the resolution of the raster data including a DEM and an orthorectified composite image is determined.

Slope distribution and topographic contour lines are derived from the DEM using GIS software (ArcGIS Desktop 10.3 by ESRI). ~~The h~~ummock bases were traced using the DEM-derived topographic data and orthorectified image as follows: First, to identify local convex mounds in the DEM, the elevation values are multiplied by -1 to generate a flip-side of the DEM, and the local depressions in the inverse surface are highlighted by applying the sink-fill process. ~~For the sink-fill~~, the D8 flow directions based on the surrounding eight cells are derived from the flip-side DEM (Jenson and Domingue, 1988), and the depressions are virtually filled up to match with the local trend surface. The filled areas roughly correspond to the local mounds in the original DEM. Second, the orthorectified ground-surface image and slope distribution are used to detect ~~the~~ boundaries of the actual mounds. Because the flat lands in the main area are mostly cultivated whereas the mounds of hummocks are unsuitable for cultivation due to their rocky composition, the boundaries of the hummock mounds ~~are clearly shown~~ in the ground-surface images. Also, the gap of slope angles is clear to separate the mounds and surrounding flatlands. Topographic contour lines are supportively used to trace the mound boundaries~~, although the~~ boundaries are not always horizontal and the contour lines ~~themselves~~ do not generally follow the mound boundaries except flat areas. Polygon vector data ~~showing the hummock mound boundaries~~ are then obtained. ~~The reliability of the mound boundaries was checked in the field for some of the hummocks.~~

The geometric features of hummocks are then examined in GIS and area is calculated for each polygon. The height of a hummock is estimated by constructing a flat ~~basement surface of each hummock by interpolating the elevation~~ values on the polygon peripherals by triangular irregular network (TIN) surface. The maximum difference between the actual surface and

the estimated basement surface is regarded as the height of the hummock. Although the actual mass of a hummock should exist in the underground areas, the depth of such the submerged structure is ~~hard to be known~~, and the surficial height of hummocks have often been utilized as a representative index showing their morphological characteristics (Glicken, 1996). The upper-half volume of a hummock, i.e., the volume of the hummock mound above the basement surface, is also obtained as one of the proximal indicators of the hummock size. The volume is calculated as the sum of the elevation differences between the actual surface and the estimated basement surface for each cell in a hummock polygon.

Relationship~~s~~ between hummock alignments and the flow direction of debris avalanche have ~~often~~ been studied~~, where the~~ orientation of hummocks is ~~the~~ key morphological measure to investigate the dynamics of debris avalanche (Glicken, 1996; Paguican et al., 2012; Yoshida, 2014). Here, two directionality indices of the polygons are calculated based on their major axis. One is the direction from the north, and another is the displacement angle against the flow direction of DAD. ~~Fig.~~ 4 shows the definition of the displacement angle of the major axis of a hummock: the angle between the main direction of the valley-filling DAD and the major axis (Yoshida, 2014). The main direction of the DAD ~~in the study site is~~ the north. The distance from the source along the valley, as explained later, is also assigned to the centroid of each polygon (Fig. 4).

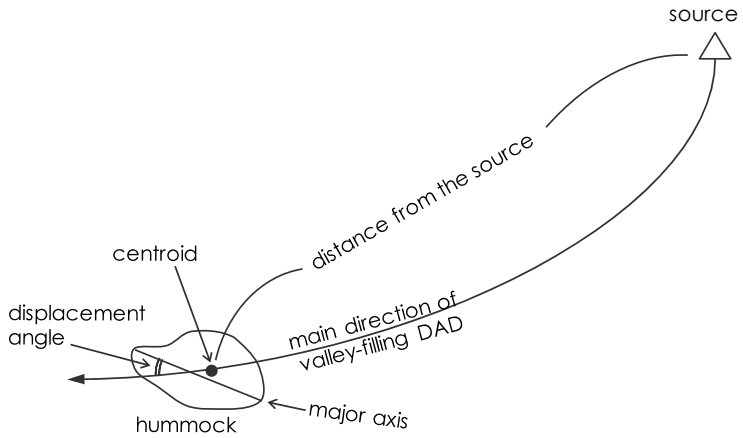

Figure 4: Definition of the displacement angle of a hummock (modified after Yoshida, 2014).

3.2. Reconstruction of the source area of DAD using PRISM-DEM

As background topographic and imagery data covering areas wider than the RPAS-derived data, we used AVNIR-2 (Advanced Visible and Near Infrared Radiometer type 2), a satellite-based imagery and PRISM (Panchromatic Remote-sensing Instrument for Stereo Mapping) mounted on ALOS (Advanced Land Observation Satellite). The AVNIR-2 sensor has four bands for visible and near-infrared wavelengths, with a typical resolution ~~is~~ 10 m. These data are too coarse for hummock extraction but can be used as a background data. The AVNIR-2 data was to confirm the hummocky topography in and around the DAD. The PRISM optical sensor is a panchromatic radiometer for wavelengths of 0.52–0.77 µm, with a spatial resolution of 2.5 m. The original data was processed to generate a 3-m resolution DEM with a vertical accuracy of ~6 m (Takaku and Tadono, 2007; Habib et al., 2017)~~, and~~ is resampled to 10 m resolution to avoid surficial noises. Although there ~~remain more errors~~ particularly around the borders of mosaic images due to ~~their~~ mismatch~~ing~~, the DEM can be used as a background topographic condition covering the whole area of the sector collapse, DAD, and surrounding areas. The resolution and accuracy of the DEM are, however, unsuitable for the extraction and analysis of small hummocks.

The PRISM-DEM was further processed to show topographic characteristics in the study site. The distances along flow paths based on the D8 flow directions are generated using the hydrological toolset in the GIS software, providing the position of the hummocks (the distance from the source) based on the flow directions (Fig. 4). The longitudinal and transverse profiles along the main course of the DAD are also obtained from the PRISM-DEM. Elevation and distance from

the source (the summit of Mt. Erciyes) are sampled at a 100-m interval along the main course of the debris avalanche for the longitudinal profile. At the same time, the maximum elevation within a 500-m length of a transverse cross section perpendicular to the flow direction is recorded for each sampling point to represent the amount of reliefs along the valley bottom. Stream gradients at different scales are calculated from the sampled elevation by averaging for 400-m and 2,000-m horizontal lengths. The 400-m scale stream gradient represents local fluctuations in the longitudinal profile, while the 2,000-m gradient reflects the trend of elevation changes along the profile. Transverse cross profiles (3,000-m long) perpendicular to the flow direction are extracted at every 1,500 m along the main course of the debris avalanche.

The original surface of mountain slopes before the sector collapse is estimated based on the shape of the surrounding slopes, assuming that the topography has not been highly modified. For this purpose, two different approaches are applied: One is a simple linear extrapolation of the original slopes in a cross profile on both sides of the sector collapse, and the other is to fit a Bézier curve to the linearly extrapolated cross profile. The linear extrapolation may result in an overestimate of the original surface, while the Bézier curve fitting may result in an underestimate. The original surface may fall within these two different reconstructions. For the linear extrapolation, the cross-section points on the surrounding slopes just behind the scars which are supposed to preserve the original topography are used as the source. The length of the cross sections for the linear fitting is defined as ~400 m, according to the preservation of slope linearity in the cross sections. The extrapolated two lines over the collapsed area from the both sides of the scar (P_0 and P_2 in Fig. 5) cross at a certain point (P_1 in Fig. 5), which is regarded as the ridge of the reconstructed original slopes.

For the quadratic Bézier curve fitting, the edge points of the surrounding slopes on both sides of the collapsed area (P_0 and P_2) are used as the endmost control points, while the intermediate control point (P_1) is given as the cross point of the two linearly-extrapolated lines (Fig. 5). The function of a quadratic Bézier curve is given as:

$$B(t) = (1-t)[(1-t)P_0 + tP_1] + t[(1-t)P_1 + tP_2] , \quad (1)$$

hence

$$B(t) = (1-t)^2 P_0 + 2(1-t)tP_1 + t^2 P_2 , \quad (2)$$

where $B(t)$ is the estimated elevation, and t represents the relative position between the points of P_0 and P_2 ($0 \le t \le 1$). Eq. (2) was applied to the multiple transverse profiles across the collapsed area (A in Fig. 1), which are set at a horizontal interval of 300 m.

Reconstruction of the original topography by linear and Bézier methods used 3-dimensional TIN models. The differences between the reconstructed TIN surface and the present land surface are calculated as the estimated volumes of the sector collapse.

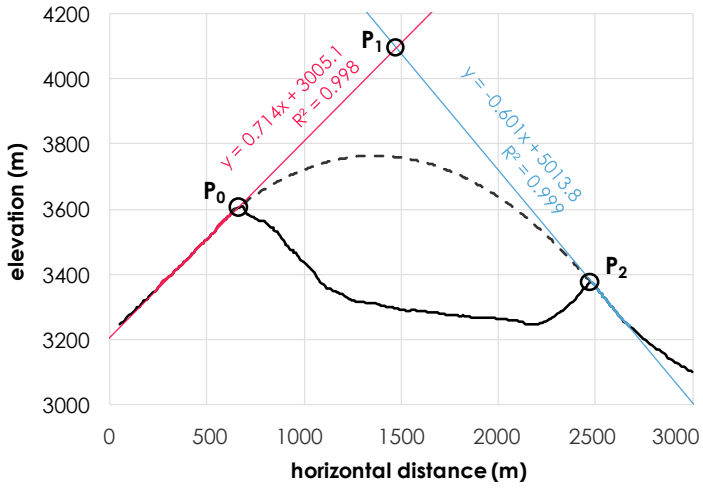

Figure 5: An example of reconstructing the original topographic surface of the sector collapse by two methods: linear extrapolation (solid red and blue lines) and Bézier curve fitting (dashed line).

4 Results

4.1 Morphometric characteristics and distribution of hummocks

There were eight UAV flights that took 2900 photos. Of these, 1572 were used for photogrammetry after excluding low-quality or misaligned images. To adjust the geographical coordinates of the tie points and camera locations, GCPs were set in the images and the tie points and camera locations were adjusted to fit the GCP-derived coordinates. ~~In the field,~~ ~~5~~ GCPs were set around the main ~~area with hummocks,~~ ~~whose~~ geographical coordinates taken by the post-processed GNSS provided positional errors of 0.31 m and 0.41 m in horizontal and vertical directions, respectively. The bundle adjustment using these GCPs resulted in the estimated horizontal and vertical accuracies of the topographic model of 0.48 and 0.99, respectively. Although the number of GCPs is not many, and the errors are on the order of decimeters, we assume that these error values are sufficiently suitable for the analysis of hummocks in 10^1–10^3 m^2 scales. After removing the points with large reprojection errors (>0.79 pixels), the number of valid tie points for the paired images was 14,220,242. The multi-view stereo photogrammetry was then performed to generate the dense point cloud of 51,505,810. Based on this three-dimensional point cloud and the original images, the data of land surface imagery and topography were obtained, covering an area of 8.5 km^2. The resolution of the raster-type topographic data (DEM) was set to be 36 cm, based on the average point density of 7.8 pts/m^2. The orthorectified image was given with a resolution of 9.0 cm, based on the average ground resolution of the original image of 8.96 cm/pix.

The outline of hummocks was then traced from the RPAS-derived topographic and image data (Fig. 6). In total, 65 hummocks were extracted, all are within ~11 to 13 km away from the DAD source. Table 1 shows the basic morphological properties of the hummocks. The polygon area ranges over two orders of magnitude from 100 m^2 to 20,000 m^2, with a mean area of ~~3315.8~~ m^2. The height shows less variation from 1 to 20 m with a mean of 5.4 m, while the volume largely ranges from 200 to 770,000 m^3 with a mean of 79,429 m^3. The lengths of major and minor axes are tens to hundreds of meters with means of ~~69.1 m and 41.4~~ m, respectively. The mean elongation ratio, i.e., the length ratio of the major axis to the minor axis, is 1.7, equivalent to an approximate aspect of 5:3.

The displacement angle (the relative orientation against the flow direction of the debris avalanche) almost fully ranges from 0° to 90°, with an average of ~~38.1~~°. Fig. 7 shows more details of the orientation and displacement of the hummocks in histograms. The north-based orientation shows large fraction toward the north (Fig. 7a), while the displacement angle shows a bimodal distribution in the histogram, with relatively large fraction around 0–40° (Fig. 7b). These indicate that many hummocks tend to follow the direction of the northward flow of the debris avalanche, but some are exceptionally placed with large displacements against the flow direction.

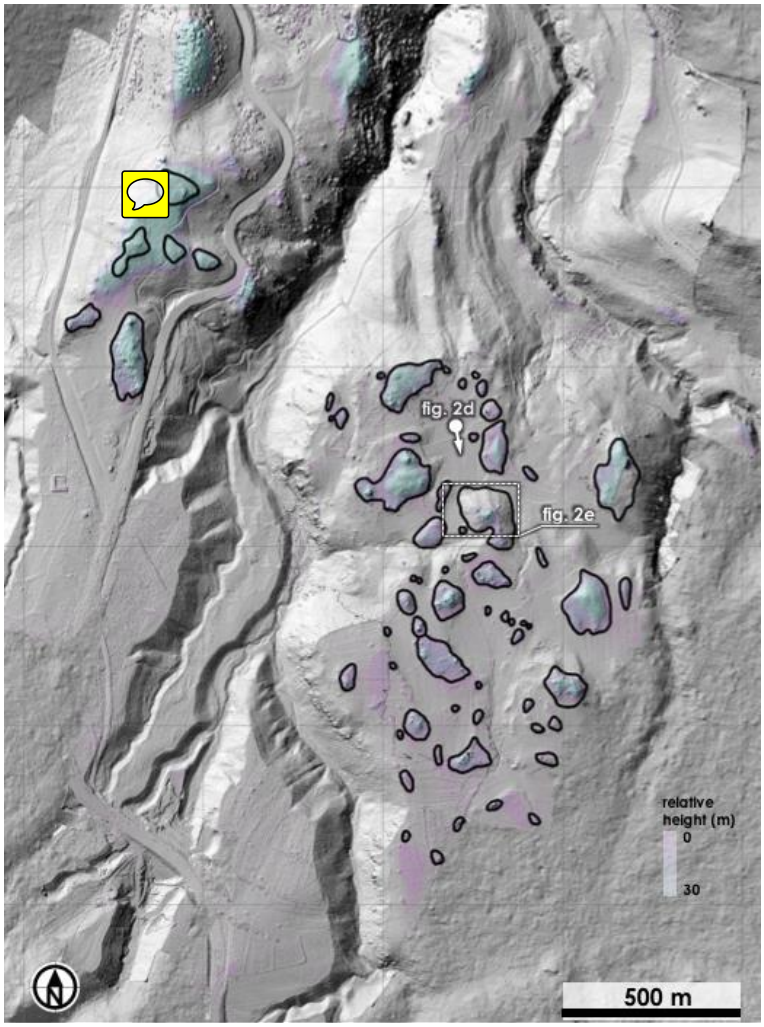

Figure 6: Map of the hummocks extracted in the study area (n = 65). Blue to purple colors show the sink-filled areas on the inverse DEM, indicating the locations of local mounds and ridges. Black solid lines represent the mound boundaries of hummocks identified. Note that not all the sink-filled areas are identified as hummocks, based on the interpretation of orthorectified images and field observations. Hillshade images are derived from RPAS-derived 36-cm DEM (foreground) and 10-m PRISM-DEM (background).

Table 1: Morphological properties of hummocks

properties of hummocks	average	minimum	maximum
distance from the source (m)	12,177	11,158	13,464
area (m^2)	3,315.8	118.3	19,615.6
top height (m)	5.4	0.9	20.1
volume (m^3)	79,429	210	774,506
major axis length (m)	69.1	13.7	240.5
minor axis length (m)	41.4	11.5	140.5
elongation ratio	1.7	1.0	3.1
displacement angle (degrees)	38.1	0.3	89.6

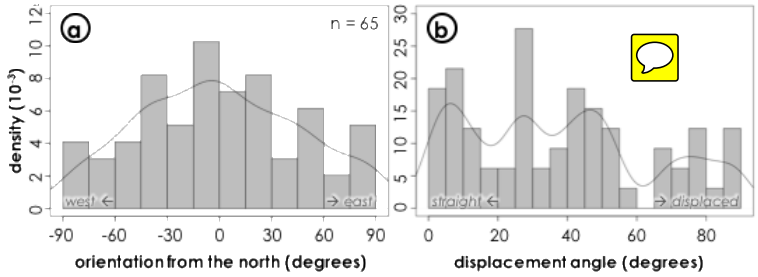

Figure 7: Horizontal angles of the direction of hummocks. (a) Orientation from the north. West is -90° and east is 90°. (b) Displacement angle, i.e., the relative orientation of the major axis of hummock polygons to the main flow direction of debris avalanche, given in 0–90°. Smaller displacement angle (straight to the flow direction) indicates extensional regime of the debris avalanche, while larger displacement angle (displaced against the flow) corresponds to the compressional regime.

Fig. 8 shows the longitudinal profile and stream gradients along the main course of the DAD derived from PRISM-DEM. The longitudinal traces of maximum elevation within 500 m from the valley center are also shown as a gray line. The differences of the maximum elevation and the bottom elevation indicate deepness of the incision in the valley bottom. With some fluctuations, both the local and trend stream gradients decrease as the distance from the source increase. The gradients are particularly low in the reach upstream of the portion where hummocks are present (around 8–12 km from the source). In this upstream reach within the caldera wall, less difference in elevations is observed for the valley bottom and nearby 500-m cross section area, representing the low relief along the stream. In contrast, the stream gradients, as well as the elevation differences, are particularly high in the downstream reach of the hummock-dominated area for approximately 5 km (13–18 km from the source). In this reach, the trend stream gradient (2,000-m scale) increases up to 0.1 m/m, while the elevation difference reaches 100–200 m. This reach corresponds to the outlet of the caldera and shows a form of the deep gorge (Fig. 2c). This can be regarded as a knickzone, which has relatively steeper gradient than the adjacent upstream and downstream reaches (Hayakawa and Oguchi, 2006).

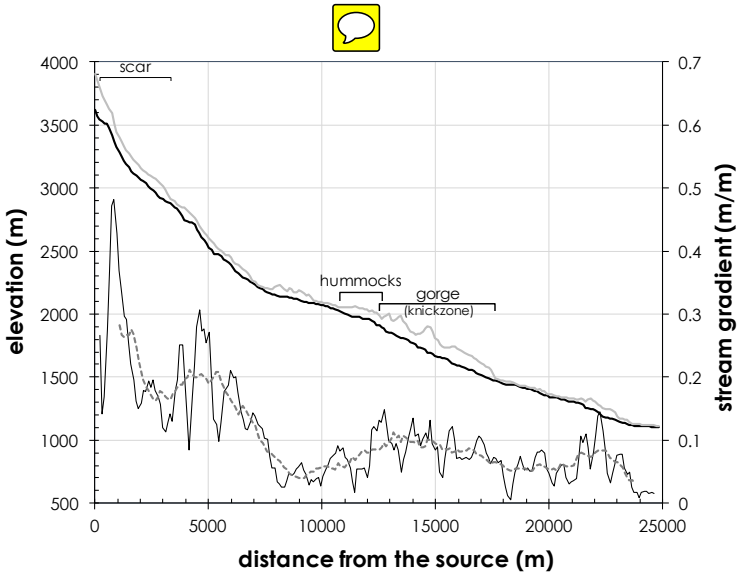

Figure 8: Longitudinal profile and stream gradient along the main course of the DAD. The black solid line in the upper side (left y-axis) indicates the longitudinal profile along the main course whose location is shown in Figure 1, while the solid gray line indicates the maximum elevation within the 500-m range across the main course. The thin black line on the lower side (right y-axis) is the stream gradient averaged for 400-m reach upstream and downstream for each sampling point, whereas the dashed gray line is that averaged for 2000-m reach.

Transverse cross profiles along the DAD extracted from PRISM-DEM show downstream widening of the DAD in elevations of 2800–2200 m, and narrowing in 2200–1600 m (Fig. 9). The potential extent of the DAD, ~~whose~~ downstream limit corresponds to the location of the northernmost outcrop identified in the field (Fig. 1), was highlighted as solid black

lines in Fig. 9. The upper part of the DAD (approximately 2800–2300 m in elevation) shows convex-up cross profiles, whereas the middle part (2300–2000 m) is more straight and flat. The downstream-most part (below 2000 m) exhibits more rugged shape by the incised valley of the knickzone reach. The hummocks are located in the transitional area (around 2000 m elevation) from the flat to the incised areas. Far downstream areas out of the DAD extent again show straight and flat transverse profiles.

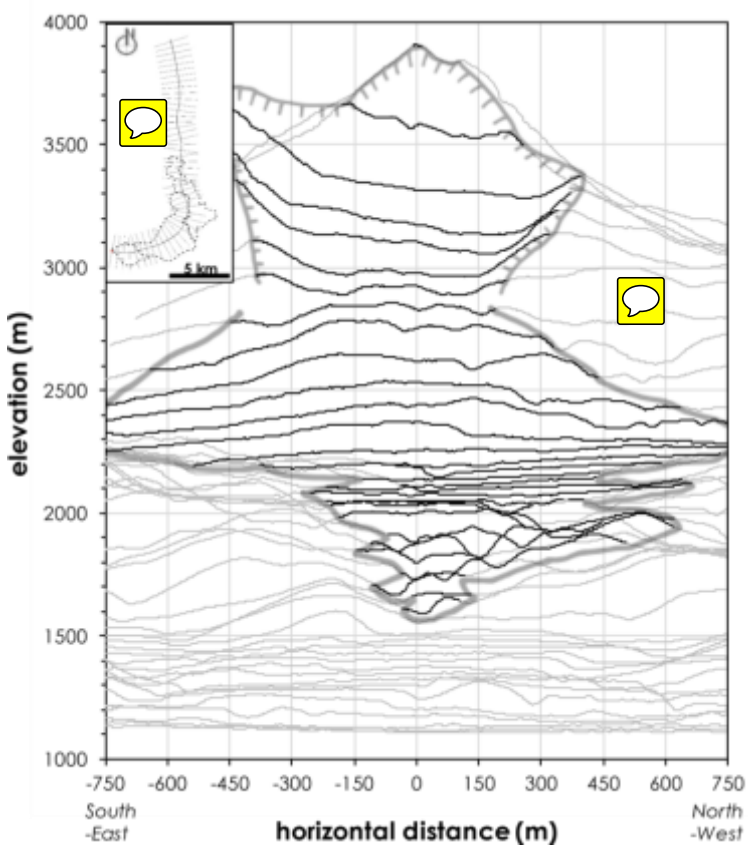

Figure 9: Transverse profiles across the DAD. Areas of the sector collapse and the potential DAD extent are shown in black surrounded by thick gray lines. Inset map (upper left) shows the location of these sections along the main course of the debris avalanche over the mapped extent of the DAD.

The area of the polygons of the hummocks was summarized for each 500-m bin of the distance from the source summit to be compared with the previously reported binned average of hummock areas along the distance (Fig. 10; Yoshida et al., 2012). In Fig. 10, the mean area of all hummocks identified for each 500-m distance is shown as white circles, whereas the mean area for all the hummocks is shown as a black horizontal bar. The limited distribution and concentration of hummocks only in the area 11–13 km from the summit and the downstream increase in hummock area suggest that the distance-size relationship does not work for Mt. Erciyes DAD.

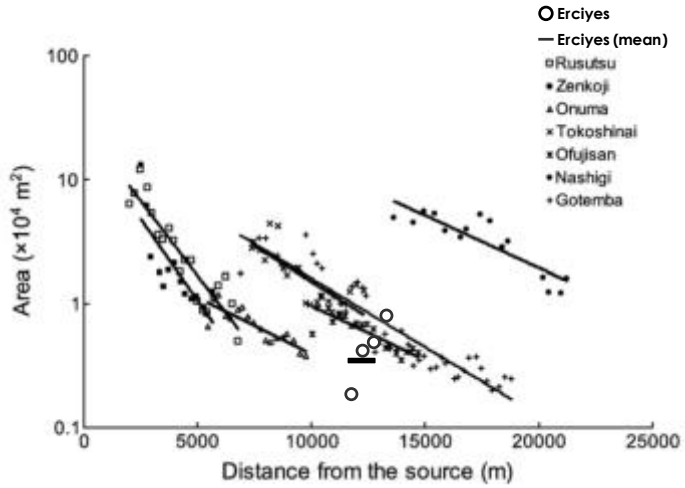

Figure 10: Relationship between the distance from the source and hummock size for the avalanche in Mt. Erciyes and those previously reported by Yoshida et al. (2012). The white circles indicate the mean area of hummock polygons summarized for each 500-m bin of the distance, while the black horizontal bar shows the average areas for all the hummocks in Erciyes. Solid lines are linear regressions for each avalanche previously reported.

4.2 Volume estimation of DAD by the source area reconstruction

Using ~~the~~ two different interpolation methods ~~by~~ linear and Bézier, the original surfaces ~~s~~ of the ~~mountain body~~ before the sector collapse were reconstructed (Figs. 11, 12). The particular difference between the linear and Bézier methods is the maximum summit elevation of the reconstructed surface. The summit ~~of the linearly interpolated original mountain body reaches~~ 4100 m ~~of~~ elevation ~~that~~ is much higher than the present summit of 3917 m (Fig. 11c), ~~while that~~ by ~~the~~ Bézier method do not exceed the present summit elevation (Fig. 11d). In ~~any case~~, the summit of the reconstructed ~~mountain body appears~~ at 1 km southeast of the current summit (Figs. 11a, b, 12b, c).

The volume of the missing ~~mountain body~~ by the sector collapse is calculated as the sum of the elevation differences between the reconstructed surface and the present landform: 12.75×10^8 m^3 by ~~the~~ linear method, and 10.67×10^8 m^3 by ~~the~~ Bézier method. Due to the preexisting dissection of the mountain before the collapse or a crater on the top, this reconstructed volume may be reduced by approximately 10% (Aramaki, 1963; Yonechi et al., 1988; Yoshida and Sugai, 2007). If this is applied, the estimated source volume of the sector collapse is given as $9.60–11.48 \times 10^8$ m^3. Since the plan area of the sector collapse source area is 5.2 km^2, the mean depth of the missing mountain body is obtained to be 186–223 m. Although the accuracy of this estimation is hard to be quantified due to the lack of any morphological evidence of the sector before the collapse, we consider these values as a feasible, order-of-magnitude estimate of the missing volume and depth.

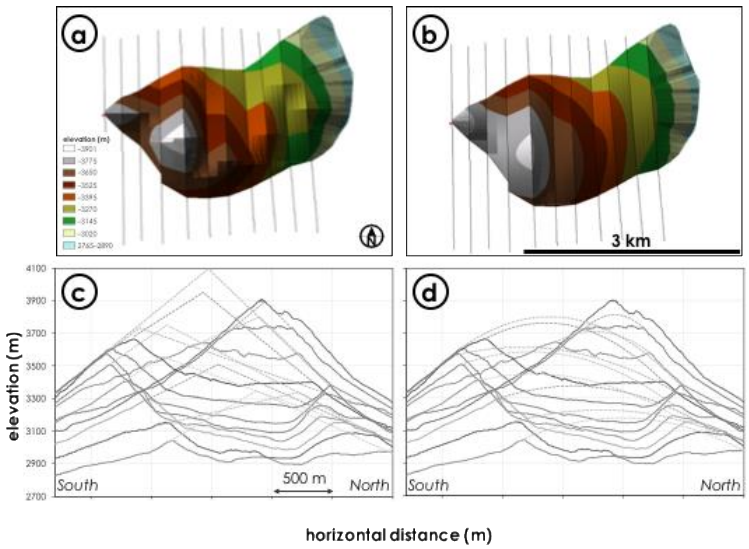

Figure 11: Reconstruction of the source area of the sector collapse. Scales are the same for a/b and c/d, respectively. (a) Plan view of the reconstructed surface by the linear method. The red triangle indicates the location of the current summit of Mt. Erciyes. (b) Plan view of the reconstructed surface by the Bézier method. (c) Transverse profiles of the original surface by the linear extrapolations. (d) Transverse profiles by Bézier curve fitting.

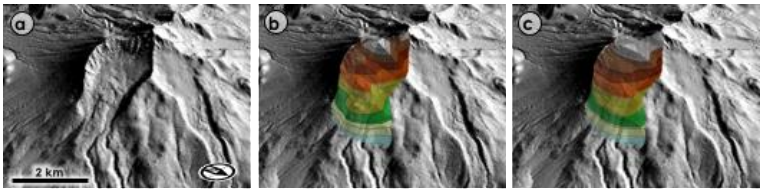

Figure 12: Bird-eye views of the reconstructed source area of the sector collapse. (a) Present topography of the scar. (b) 3D TIN of reconstructed surface of the original mountain body by linear extrapolations. (c) 3D TIN of reconstructed surface of the original mountain body by Bézier curve fitting.

5 Discussion

5.1 Characteristics of the debris avalanche inferred from the volume and thickness

Because of the expansion of the original mass ~~and~~ sediment entrainment during ~~its~~ transport, the volume of DAD ~~may be larger~~ than that of the missing sector for 25–30% (Siebert, 1984; Yoshida and Sugai, 2007). Accounting for the estimated source volume of 9.6–11.5 × 10^8 m^3, the potential volume of the DAD would become 12–15 × 10^8 m^3. This estimated volume is relatively larger than the average volume (ca. 5 × 10^8 m^3) of reported DADs in the Holocene and Pleistocene (Siebert, 1984), but falls within the range of 2–260 × 10^8 m^3 (Siebert, 1984). If compared with the known cases, the estimated volume is comparable to the debris avalanche in the historical time period at Mt. Iriga in the Philippines, whose volume is known as 15 × 10^8 m^3 (Aguila et al., 1986; Paguican et al., 2012), and more than half of that of the Mt. St. Helens case ~~in~~ 1980 ~~as 25–28 × 10^8 m^3~~ (Voight et al., 1983; Siebert et al., 1987; Glicken, 1996). Also, the estimated volume of Erciyes is approximately twice or three times of the well-described case of the northern flank of Mt. Bandai ~~(Japan)~~ in 1888 triggered by a phreatic eruption ~~(4.9 × 10^8 m^3)~~ (Yonechi et al., 1988; Yonechi and Chiba, 1989; Yoshida, 2012), or the non-eruptive case of Mt. Unzen-Mayuyama ~~(~~Japan~~)~~ in 1792 (4.4 × 10^8 m^3) (Inoue, 1999; Takarada and Melendez, 2006).

Although the exact extent of the DAD is ~~hard to be clarified~~ in this study, the rough estimation of the potential extent of the DAD in this study has an area of at least 20 km^2, which is apparently larger than that (14 km^2) previously mapped by Şen et al. (2003). Dividing the estimated source volume of the DAD, 12–15 × 10^8 m^3, by the potential extent of the depositional area of 20 km^2, the mean thickness of the DAD is ~60–75 m. This thickness of DAD is much larger than those reported in the previous studies: e.g., 25–30 m for Mt. Asama (Yoshida and Sugai, 2010), 45 m for Mt. St. Helens (Voight et al., 1983).

The area and volume of the DADs across the world summarized by Siebert (1984) also gives an average thickness of 24 m with a range of 3–58 m, Mt. Erciyes for DAD thickness is out of the range of the reported ones. This supports that the extent of the depositional area of the DAD of Mt. Erciyes can be much larger than 20 km^2, potentially twice to three-times of the identified area. ~~Although the sedimentary evidence is not available, the debris avalanche could have flown downstream over the gorge and spread over the relatively flat area farther than 18 km from the source summit (Fig. 8) where elevation is lower than ~1500 m (Fig. 9).~~

5.2 Debris avalanche and formation of hummocks

Based on the plots in Fig. 10, the distance-size relationship for Erciyes may be comparable to the case of the Onuma avalanche on Komagatake volcano, the Ofujisan avalanche on Nasu volcano, or the Gotenba debris avalanche on Mt. Fuji (Yoshida et al., 2012). However, unlike the other cases, the Erciyes hummocks are densely found only in a limited area (11–13 km from the source). The distance-size relationship of hummocks cannot be directly compared to the other cases in which hummocks are more evenly distributed (Siebert, 1984; Yoshida et al., 2012).

In turn, the absence of hummocks in both upstream and downstream reaches indicate a different pattern of debris avalanche flow for this particular case of Mt. Erciyes. In general, hummocks in DADs are primarily formed due to the initial stage of sliding of the original sector of the mountain body, with some blocks preserving the original structure that appears as secondary hummocks by floating on the surface of DADs in the later stage (Paguican et al., 2014). In the upstream reach of the present hummocks of Mt Erciyes, the absence of such primary hummocks in the 0–11 km area from the source may indicate either that hummocks are not formed due to the high fracturing of DADs, or that hummocks are formed but buried by subsequent sediment covering over the DAD.

On one hand, such ~~the~~ high fracturing of the Erciyes DAD is feasible because the debris avalanche could have had low viscosity with high water content with a sufficient amount of ice of glaciers on the original mountain in the glacial period, likely under the cool and wet climate in the late Pleistocene (Sarıkaya et al., 2009; Bayer Altin et al., 2015). It should also be noted that the debris avalanche flow was affected by the pre-existing topography of the former caldera (Fig. 1). The debris avalanche is supposed to have initially flown to the east, and after blocked by the former caldera wall located in the east, the debris avalanche changed its direction to the north (Fig. 1). If the debris avalanche is well fractured, the flow could have shallowly spread over the flat area within the caldera without forming primary hummocks.

On the other hand, even if some small primary hummocks were formed at the initial stage, they could have been hidden by post-collapse modifications and surficial sediment deposition in this upstream area of the DAD (Yoshida and Sugai, 2007), as indicated by the presence of convex-up cross profiles in elevation of 2800–2300 m (Fig. 9, or around the letter B in Fig. 1). Although no significant eruptive activity producing thick tephra or pyroclastic flows has been recognized in the volcanic stratigraphy (Şen et al., 2003), post-collapse eruptive activities including pyroclastic flows might have occurred at a more local scale to cover the upper portion of the DAD. Loose materials including volcanic colluvial or alluvial deposits on the surrounding slopes could also have been reworked to contribute to cover the DAD. However, the thickness of such surficial sediment remains to be examined.

In the downstream reach of the present hummocks, the stream gradient is high, and the valley width is narrow forming a knickzone (Figs. 8, 9). This topographic feature could have existed before the sector collapse because this location corresponds to the intersection of the north-oriented valley, which seems to follow the mapped fault line as discussed later, and the former caldera wall of the pre-Erciyes volcanic activity (Fig. 1). The debris avalanche went over the wall at this pre-existed narrow outlet valley in the north. At the entrance of this narrow outlet valley, however, the flow might be slower as it entered the valley over the caldera. The secondary hummocks that are presently observed could have been placed around this terminal portion of the caldera floor due to the confinement of the sliding materials. The flow could then have acquired higher speed when flowing through the steepened reach of the knickzone. The bimodal distribution of the displacement angle

of hummocks would support this hypothesis (Fig. 7b). As suggested by the displacement angles, some hummocks with displaced orientations indicate a partial compressional regime of the debris avalanche: The sliding materials are confined, and hummocks are emplaced with their major axis perpendicular to the flow direction (Paguican et al., 2014; Yoshida, 2014). Whereas, the other hummocks without large displacements indicate an extensional regime of the debris avalanche due to the rapid northward flow through the valley: the stretch of the materials forced some of the hummocks aligned to the flow direction (Paguican et al., 2014; Yoshida, 2014). Such a change in the flow regime of debris avalanche can also be supported by progressive changes in flow materials (Clavero et al., 2002). In this case, since the debris avalanche flowed in the caldera, the increase in water content of the avalanche bottom is feasible if there was a caldera lake or rivers prior to the collapse. The lowering of friction at the bottom flow could have enhanced the rapid passage through the valley, while the avalanche surface remained dry enough to emplace the hummocks.

The debris avalanche materials which went over the gorge could have been further deformed and shallowly spread over the relatively flat area after reaching the downstream of the knickzone (Figs. 8, 9). Hummocks may no longer be formed in such highly-fractured materials of the debris avalanche. No data on the detailed geological structure in the downstream areas is available, and it is hard to find the extent of the DAD. Further careful investigations regarding the remnant of this DAD would be required to clarify the actual impact of the debris avalanche in this region. Moreover, such a complex case of debris avalanche with both topographic barriers (caldera wall) and passage (valley) has not frequently been reported in the previous studies, except for a few cases (Francis et al., 1985; Yoshida and Sugai, 2015). The case of Erciyes remarks the necessity of considering complex topographic constraints for the prediction of flow dynamics of debris avalanche.

5.3 Potential effects of fault lines on the debris avalanche

The presence of the strike-slip Erciyes Fault (Fig. 1) may have affected the debris avalanche. Although the exact age and intensity of the fault activity are unknown, and the presence of the fault itself also needs further careful assessments (Okumura et al., 2016), the regional stress field related to this fault group could have affected the occurrence and the direction of the sector collapse of Mt. Erciyes. In general, sector collapses often occur in the direction perpendicular to the major horizontal compression by faulting beneath the volcano (Moriya, 1980; Siebert, 1984; Vidal and Merle, 2000; Tibaldi et al. 2008), or in parallel to the fault directions (Lagmay et al., 2000; Yokoyama and Nakagaki, 2003; Wooler et al., 2009). In Mt. Erciyes, the major horizontal compression by the strike-slip faults in the north-south direction could have caused the sector collapse toward the east. Furthermore, the northward valley seems to have been formed along the fault line cutting the caldera wall. The debris avalanche, which has flown to the north being blocked by the pre-existed caldera wall, could have spread far downstream by overpassing the former caldera wall along the pre-existed valley. In such a case, the existence of local faults has dual significance, in the occurrence of sector collapse itself, and in the directionality of the debris avalanche. Although further examination of this issue are out of the scope of this study, detailed surveys of active faults and stress field in this region is also highly significant in predicting the future sector collapse of the volcano (Tibaldi et al. 2008; Wooler et al., 2009).

6 Conclusions

In this study, we utilized the RPAS-based SfM-MVS photogrammetry to map the topography of Mt. Erciyes DAD. Detailed outlines of hummocks were extracted from the high-definition land surface data. Despite the limited availability of high-definition aerial or satellite images, rapid on-site acquisition by RPAS-based SfM-MVS photogrammetry enabled to obtain new insights regarding the formation of hummocks and DAD at Mt. Erciyes. The volume of the sector collapse was estimated by reconstructing the original topography of the source area. Although the precise extent of the DAD is difficult to trace, the estimated volume of ~12–15 $\times$ 10^8 m^3 suggests that considerable amount of sediment could have spread

downstream over the observed limit of the DAD. Morphological analysis of the extracted hummocks suggests that the geometry of the hummocks in this study area is characterized by pre-existing topographic constraints, which significantly controlled dynamics of debris avalanche emplacement and formation of hummocks. In particular, former caldera walls had a strong effect on the flow direction of the debris avalanche as it confined the flow. The presence of strike-slip fault can also have considerable effects on both the occurrence of the sector collapse and the flow path of the debris avalanche. Such factors as pre-existing topographic and tectonic characteristics should carefully be considered for the hazard estimation of sector collapses, which can occur in many places ~~over~~ the world.

The study area is one of the potentially hazardous areas in the East Anatolian Fault zone with densely distributed volcanoes and faults (Koçyiğit and Erol, 2001; Korkmaz, 2009; Okumura et al., 2017). Such ~~the~~ activities of active faults (earthquakes) and volcanoes themselves are hazardous, and they can trigger ~~the~~ sector collapse and succeeding debris avalanche in the area. The detailed map of the DAD should be incorporated into a regional geomorphological map to be further examined ~~together with~~ other geomorphological features including fluvial valleys, terraces, lakes and active faults (Erol, 1999). In particular, the insights inferred from this study proposes the necessity of the assessment of potential debris avalanche paths. As noted, the studied debris avalanche had been significantly affected by topographic constraints, and the flow path was relatively limited following the pre-existing topographic slot across the caldera. This means that the hazardous areas affected by debris avalanche are rather limited, regardless of the direction of the initial collapse of the mountain body. Further investigations such as numerical modeling of the debris avalanche flow based on the present topography are expected to be carried out. At least, several scenarios of the potential sector collapse of the present mountain body should be proposed in the future studies.

In addition, although the age of the sector collapse is relatively old (possibly 20–80 ka; Şen et al., 2003; Sarıkaya et al., 2009), subsequent sediment supply from the DAD could also have affected ancient human activities in the Holocene period in the downstream basin areas. Since a lot of archaeological sites are found and investigated in the area (Kontani et al., 2014; Yener et al., 2015), the assessments of the relationships between DAD and surrounding palaeoenvironments including human activities will provide further insights for the potential disaster and its mitigation in the study area, such as floods, volcanism, landslides and fault-induced earthquakes.

Acknowledgements

We would like to thank Prof. Dr. Fikri Kulakoğlu for his fundamental assistance throughout the field work. This work is supported by JSPS KAKENHI Grant Number JP26560153 and JP25702014, and by JSPS Bilateral Programs Joint Research Projects. This work is a part of Joint Research by CSIS, The University of Tokyo.

References

Aguila, L. C., Newhall, C. G., Miller, C. D. and Listanco, E. L.: Reconnaissance geology of a large debris avalanche from Iriga volcano, Philippines, Philipp. J. Volcanol., 3, 54–72, 1986.

Aramaki, S.: Geology of Asama volcano, J. Fac. Sci. Univ. Tokyo, Sect. II, 14, 229–443, 1963.

Bayer Altin, T., El Ouahabi, M. and Fagel, N.: Environmental and climatic changes during the Pleistocene–Holocene in the Bor Plain, Central Anatolia, Turkey, Palaeogeogr. Palaeoclimatol. Palaeoecol., 440, 564–578, doi:10.1016/j.palaeo.2015.09.011, 2015.

Bernard, B., van Wyk de Vries, B., Barba, D., Leyrit, H., Robin, C., Alcaraz, S. and Samaniego, P.: The Chimborazo sector collapse and debris avalanche: Deposit characteristics as evidence of emplacement mechanisms, J. Volcanol. Geotherm. Res., 176(1), 36–43, doi:10.1016/j.jvolgeores.2008.03.012, 2008.

Clavero, J., Sparks, R., Huppert, H. and Dade, W.: Geological constraints on the emplacement mechanism of the Parinacota debris avalanche, Northern Chile, Bull. Volcanol., 64(1), 40–54, doi:10.1007/s00445-001-0183-0, 2002.

Dufresne, A. and Davies, T. R.: Longitudinal ridges in mass movement deposits, Geomorphology, 105(3–4), 171–181, doi:10.1016/j.geomorph.2008.09.009, 2009.

Emre, Ö., Duman, T. Y., Özalp, S., Elmaci, H. and Olgun, S.: 1:250,000 Scale Active Fault Map Series of Turkey, Kayseri (NJ36-8) Quadrange, Ankara., 2011.

Erol, O.: A geomorphological study of the Sultansazliği lake, central Anatolia, Quat. Sci. Rev., 18(4–5), 647–657, doi:10.1016/S0277-3791(98)00102-4, 1999.

Fonstad, M. A., Dietrich, J. T., Courville, B. C., Jensen, J. L. and Carbonneau, P. E.: Topographic structure from motion: a new development in photogrammetric measurement, Earth Surf. Process. Landforms, 38(4), 421–430, doi:10.1002/esp.3366, 2013.

Francis, P. W., Gardeweg, M., Ramirez, C. F. and Rothery, D. A.: Catastrophic debris avalanche deposit of Socompa volcano, northern Chile., Geology, 13(9), 600–603, doi:10.1130/0091-7613(1985)13<600:CDADOS>2.0.CO;2, 1985.

Glicken, H.: Rockslide-debris avalanche of may 18, 1980, Mount St. Helens volcano, Washington., 1996.

Hashimoto, N., Isoyama, K., Kuboki, J., Okumi, S. and Ozawa, A.: A geomorphological study of Iwaki volcano – particularly on the Akakurazawa mudflow hills (in Japanese with English abstract), Bull. Geol. Surv. Japan, 30, 369–377, 1979.

Habib, A., Akdim, N., El Ghandour, F. ezzahra, Labbassi, K., Khoshelham, K. and Menenti, M.: Extraction and accuracy assessment of high-resolution DEM and derived orthoimages from ALOS-PRISM data over Sahel-Doukkala (Morocco), Earth Sci. Informatics, 10(2), 197–217, doi:10.1007/s12145-017-0287-5, 2017.

Hayakawa, Y. S. and Oguchi, T.: DEM-based identification of fluvial knickzones and its application to Japanese mountain rivers, Geomorphology, 78, 90–106, doi:10.1016/j.geomorph.2006.01.018, 2006.

Hayakawa, Y. S., Obanawa, H., Saito, H. and Uchiyama, S.: Geomorphological applications of Structure-from-Motion Multi-View Stereo photogrammetry: A review (in Japanese with English abstract), Trans. Japanese Geomorphol. Union, 37(3), 321–343, 2016.

Hayakawa, Y. S., Yoshida, H., Dragut, L. and Oguchi, T.: Automated extraction of hummocks in debris avalanche deposits using DEMs: A case study at Mt. Gassan, northwest Japan, Zeitschrift für Geomorphol., doi:10.1127/zfg_suppl/2017/0361, *in press*.

Innocenti, F., Mazzuoli, R., Pasquarè, G., Radicati Di Brozolo, F. and Villari, L.: The Neogene calcalkaline volcanism of Central Anatolia: geochronological data on Kayseri—Nigde area, Geol. Mag., 112(4), 349, doi:10.1017/S0016756800046744, 1975.

Inoue, K.: Shimabara-Shigatusaku earthquake and topographic changes by Shimabara catastrophe in 1792 (in Japanese with English abstract), J. Japan Soc. Eros. Control Eng., 52(4), 59–69, 2000.

Jenson, S. K. and Domingue, J. O.: Extracting topographic structure from digital elevation data for geographic information system analysis, Photogramm. Eng. Remote Sensing, 54(11), 1593–1600, doi:0099-1112/88/5411-1593$02.25/0, 1988.

Koarai, M., Sato, H. P., Araiba, K., Osanai, N. and Itoh, H.: Geomorphological study of the Leyte debris avalanche using satellite imagery remote sensing (in Japanese with English abstract), J. Japan Landslide Soc., 45, 106–117, 2008.

Koçyiğit, A. and Erol, O.: A tectonic escape structure: Erciyes pull-apart basin, Kayseri, central Anatolia, Turkey, Geodin. Acta, 14(1–3), 133–145, doi:10.1080/09853111.2001.11432439, 2001.

Kontani, R., Sudo, H., Yamaguchi, Y., Hayakawa, Y. S. and Odaka, T.: An Archaeological Survey in the Vicinity of Kültepe, Kayseri Province, Turkey, in Current Research at Kültepe-Kanesh: An Interdisciplinary and Integrative Approach to Trade Networks, Internationalism, and Identity, edited by L. Atici, F. Kulakoğlu, G. Barjamovic, and A. Fairbairn, pp. 95–106, Lockwood Press, Atlanta, 2014.

Korkmaz, K. A.: Earthquake disaster risk assessment and evaluation for Turkey, Env. Geol, 57, 307–320, doi:10.1007/s00254-008-1439-1, 2009.

Kuzucuoglu, C., Bertaux, J., Black, S., Denefle, M., Fontugne, M., Karabiyikoglu, M., Kashima, K., Limondin-Lozouet, N., Mouralis, D. and Orth, P.: Reconstruction of climatic changes during the Late Pleistocene, based on sediment records from the Konya Basin (Central Anatolia, Turkey), Geol. J., 34(1–2), 175–198, doi:10.1002/(sici)1099-1034(199901/06)34:1/2<175::aid-gj820>3.3.co;2-d, 1999.

Lagmay, A. M. F., van Wyk de Vries, B., Kerle, N. and Pyle, D. M.: Volcano instability induced by strike-slip faulting, Bull. Volcanol., 62(4–5), 331–346, doi:10.1007/s004450000103, 2000.

Mizuno, Y.: Geomorphology of Okinajima mud flow area, special reference to mud flow hills (in Japanese), Ann. Tohoku Geogr. Assoc., 11(1), 22–24, 1958.

Moriya, I.: "Bandaian Eruption" and landforms associated with it (in Japanese with English abstract), in Collection of articles in memory of retirement of Prof. K. Nishimura from Tohoku Univ., pp. 214–219., 1980.

Moriya, I.: Geomorphological development of Bandai volcano (in Japanese with English abstract), J. Geogr. (Chigaku Zasshi), 97(4), 293–300, doi:10.5026/jgeography.97.4_293, 1988.

Nakamura, Y.: Geology and petrology of Bandai and Nekoma volcanoes, Sci. Reports, TohokuUniversity, 3(14), 67–119, 1978.

Obanawa, H., Hayakawa, Y., Saito, H. and Gomez, C.: Comparison of DSMs derived from UAV-SfM method and terrestrial laser scanning (in Japanese with English abstract), J. Japan Soc. Photogramm. Remote Sens., 53(2), 67–74, doi:10.4287/jsprs.53.67, 2014.

Okumura, K., Hayakawa, Y. S., Kontani, R. and Kulakoglu, F.: Quaternary activity of the Erciyes Fault southeast of the Kayseri Basin, Turkey, in Abstracts, American Geophysical Union 2016 Fall Meeting, T41B–2918., 2016.

Orton, G. J.: Volcanic environments, in Sedimentary environments, edited by H. G. Reading, pp. 485–567, Blackwell Science., 1996.

Paguican, E. M. R., van Wyk de Vries, B. and Lagmay, A. M. F.: Volcano-tectonic controls and emplacement kinematics of the Iriga debris avalanches (Philippines), Bull. Volcanol., 74(9), 2067–2081, doi:10.1007/s00445-012-0652-7, 2012.

Paguican, E. M. R., van Wyk de Vries, B. and Lagmay, A. M. F.: Hummocks: how they form and how they evolve in rockslide-debris avalanches, Landslides, 11(1), 67–80, doi:10.1007/s10346-012-0368-y, 2014.

Pickarski, N., Kwiecien, O., Djamali, M. and Litt, T.: Vegetation and environmental changes during the last interglacial in eastern Anatolia (Turkey): A new high-resolution pollen record from Lake Van, Palaeogeogr. Palaeoclimatol. Palaeoecol., 435, 145–158, doi:10.1016/j.palaeo.2015.06.015, 2015.

Sarıkaya, M. A., Zreda, M. and Çiner, A.: Glaciations and paleoclimate of Mount Erciyes, central Turkey, since the Last Glacial Maximum, inferred from 36Cl cosmogenic dating and glacier modeling, Quat. Sci. Rev., 28(23–24), 2326–2341, doi:10.1016/j.quascirev.2009.04.015, 2009.

Şen, E., Kürkcüoglu, B., Aydar, E., Gourgaud, A. and Vincent, P. M.: Volcanological evolution of Mount Erciyes stratovolcano and origin of the Valibaba Tepe ignimbrite (Central Anatolia, Turkey), J. Volcanol. Geotherm. Res., 125(3–4), 225–246, doi:10.1016/S0377-0273(03)00110-0, 2003.

Shea, T. and van Wyk de Vries, B.: Structural analysis and analogue modeling of the kinematics and dynamics of rockslide avalanches, Geosphere, 4(4), 657, doi:10.1130/GES00131.1, 2008.

Siebert, L.: Large volcanic debris avalanches: Characteristics of source areas, deposits, and associated eruptions, J. Volcanol. Geotherm. Res., 22(3–4), 163–197, doi:10.1016/0377-0273(84)90002-7, 1984.

Siebert, L.: Threats from debris avalanches, Nature, 356(6371), 658–659, doi:10.1038/356658a0, 1992.

Siebert, L., Glicken, H. and Ui, T.: Volcanic hazards from Bezymianny- and Bandai-type eruptions, Bull. Volcanol., 49(1), 435–459, doi:10.1007/BF01046635, 1987.

Takaku, J. and Tadono, T.: DSM and ORI generation using PRISM (in Japanese with English abstract), J. Remote Sens. Soc. Japan, 27(4), 372–385, 2007.

Takarada, S. and Melendez, C.: Depositional features and transport mechanism of debris avalanches: the 1980 Mount St. Helens, Usu Zenkoji, and 1792 Unzen Mayuyama Debris Avalanches, in Abstract, 17th International Sedimentological Congress, edited by K. Hoyanagi, O. Takano, and K. Kano, p. O–152, Fukuoka., 2006.

Tibaldi, A., Corazzato, C., Kozhurin, A., Lagmay, A. F. M., Pasquarè, F. A., Ponomareva, V. V., Rust, D., Tormey, D. and Vezzoli, L.: Influence of substrate tectonic heritage on the evolution of composite volcanoes: Predicting sites of flank eruption, lateral collapse, and erosion, Glob. Planet. Change, 61(3–4), 151–174, doi:10.1016/j.gloplacha.2007.08.014, 2008.

Tibaldi, A. and Vezzoli, L.: A new type of volcano flank failure: The resurgent caldera sector collapse, Ischia, Italy, Geophys. Res. Lett., 31(14), 2–5, doi:10.1029/2004GL020419, 2004.

Ui, T.: Origin of so-called "mud-flow deposit" at northwestern slope of Gassan Volcano (in Japanese), Bull. Volcanol. Soc. Japan Second Ser., 20(2), 110, 1975.

Ui, T.: Volcanic dry avalanche deposits — Identification and comparison with nonvolcanic debris stream deposits, J. Volcanol. Geotherm. Res., 18(1–4), 135–150, doi:10.1016/0377-0273(83)90006-9, 1983.

Ui, T., Takarada, S. and Yoshimoto, M.: Debris avalanches, in Encyclopedia of Volcanoes, edited by H. Sigurdsson, B. F. Houghton, S. R. McNutt, H. Rymer, and J. Stix, pp. 617–626, Academic Press, San Diego., 2000.

Ui, T., Yamamoto, H. and Suzuki-Kamata, K.: Characterization of debris avalanche deposits in Japan, J. Volcanol. Geotherm. Res., 29(1–4), 231–243, doi:10.1016/0377-0273(86)90046-6, 1986.

Vallance, J. W. and Scott, K. M.: The Osceola Mudflow from Mount Rainier: Sedimentology and hazard implications of a huge clay-rich debris flow, Bull. Geol. Soc. Am., 109(2), 143–163, doi:10.1130/0016-7606(1997)109<0143:TOMFMR>2.3.CO;2, 1997.

Vallance, J. W., Siebert, L., Rose, W. I., Girón, J. R. and Banks, N. G.: Edifice collapse and related hazards in Guatemala, J. Volcanol. Geotherm. Res., 66(1–4), 337–355, doi:10.1016/0377-0273(94)00076-S, 1995.

Vidal, N. and Merle, O.: Reactivation of basement faults beneath volcanoes: A new model of flank collapse, J. Volcanol. Geotherm. Res., 99(1–4), 9–26, doi:10.1016/S0377-0273(99)00194-8, 2000.

Voight, B., Janda, R. J., Glicken, H. and Douglass, P. M.: Nature and mechanics of the Mount St Helens rockslide-avalanche of 18 May 1980, Géotechnique, 33(3), 243–273, doi:10.1680/geot.1983.33.3.243, 1983.

Westoby, M. J., Brasington, J., Glasser, N. F., Hambrey, M. J. and Reynolds, J. M.: "Structure-from-Motion" photogrammetry: A low-cost, effective tool for geoscience applications, Geomorphology, 179, 300–314, doi:10.1016/j.geomorph.2012.08.021, 2012.

Wooller, L., van Wyk de Vries, B., Cecchi, E. and Rymer, H.: Analogue models of the effect of long-term basement fault movement on volcanic edifices, Bull. Volcanol., 71(10), 1111–1131, doi:10.1007/s00445-009-0289-3, 2009.

Yener, K. A. A., Kulakoğlu, F., Yazgan, E., Kontani, R., Hayakawa, Y. S., Joseph, W., Dardeniz, G., Öztürk, G., Johnson, M., Kaptan, E., Hacar, A., Yener, K. A. A., Kulako, F., Yazgan, E., Kontani, R., Hayakawa, Y. S., Lehner, J. W., Dardeniz, G., Johnson, M., Kaptan, E., Hacar, A., Kulakoglu, F., Yazgan, E., Kontani, R., Hayakawa, Y. S., Lehner, J. W., Dardeniz, G., Öztürk, G., Johnson, M., Kaptan, E. and Hacar, A.: New tin mines and production sites near Kültepe in Turkey: a third-millennium BC highland production model, Antiquity, 89(345), 596–612, doi:10.15184/aqy.20, 2015.

Yokoyama, S. and Nakagaki, Y.: Directional relation between large-scale slope failures of volcanic edifices and regional stress field (in Japanese with English abstract), J. Japan Landslide Soc., 40(1), 39–45, 2003.

Yonechi, F. and Chiba, N.: Volume of slope failure by Mt. Bandai eruption in 1888 and burial of Ura-Bandai area (in Japanese), Trans. Japanese Geomorphol. Union, 10, 72, 1989.

Yonechi, F., Chiba, N., Ozawa, A. and Ishimaru, S.: Large scale slope failure caused by Mt. Bandai's eruption in 1888 (in Japanese), in Abstracts of the 27th Annual Meeting of the Japan Landslide Society, pp. 20–21., 1988.

Yoshida, H.: Evaluation of sector-collapse volume of Bandai Volcano in 1888, Japan, in terms of size-distance distribution pattern of debris avalanche hummocks (in Japanese with English abstract), Trans. - Japanese Geomorphol. Union, 33(1), 45–60, 2012.

Yoshida, H.: Decrease of size of hummocks with downstream distance in the rockslide-debris avalanche deposit at Iriga volcano, Philippines: similarities with Japanese avalanches, Landslides, 10(5), 665–672, doi:10.1007/s10346-013-0414-4, 2013.

Yoshida, H.: Hummock alignment in Japanese volcanic debris avalanches controlled by pre-avalanche slope of depositional area, Geomorphology, 223, 67–80, doi:10.1016/j.geomorph.2014.06.024, 2014.

Yoshida, H. and Sugai, T.: Morphological characteristics of hummocks originating from the 24ka sector collapse event of Asama Volcano, Central Japan (in Japanese with English abstract), J. Geogr. (Chigaku Zasshi), 115(5), 638–646, doi:10.5026/jgeography.115.5_638, 2006.

Yoshida, H. and Sugai, T.: Magnitude of the sediment transport event due to the Late Pleistocene sector collapse of Asama volcano, central Japan, Geomorphology, 86(1–2), 61–72, doi:10.1016/j.geomorph.2006.08.006, 2007.

Yoshida, H. and Sugai, T.: Quantitative Examination of Hummock Alignment in Debris Avalanche Deposits: Zenkoji Debris Avalanche, Usu Volcano, Japan, Geogr. Rev. Japan Ser. B, 83(1), 64–72, doi:10.4157/geogrevjapanb.83.64, 2010.

Yoshida, H., Sugai, T. and Ohmori, H.: Size–distance relationships for hummocks on volcanic rockslide-debris avalanche deposits in Japan, Geomorphology, 136(1), 76–87, doi:10.1016/j.geomorph.2011.04.044, 2012.

Zernack, A. V., Procter, J. N. and Cronin, S. J.: Sedimentary signatures of cyclic growth and destruction of stratovolcanoes: A case study from Mt. Taranaki, New Zealand, Sediment. Geol., 220(3), 288–305, doi:10.1016/j.sedgeo.2009.04.024, 2009.

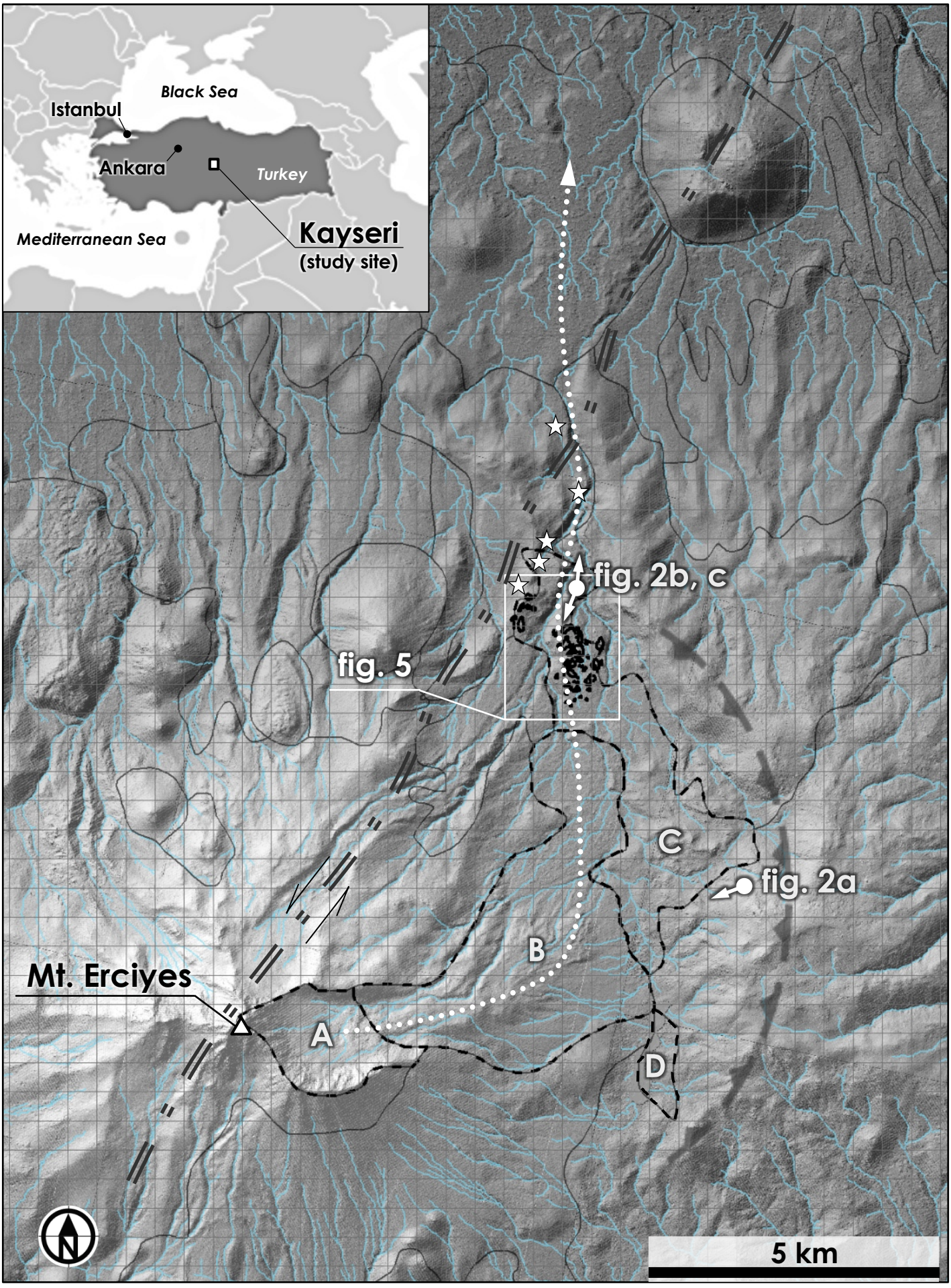

Hayakawa et al. Figure 1.

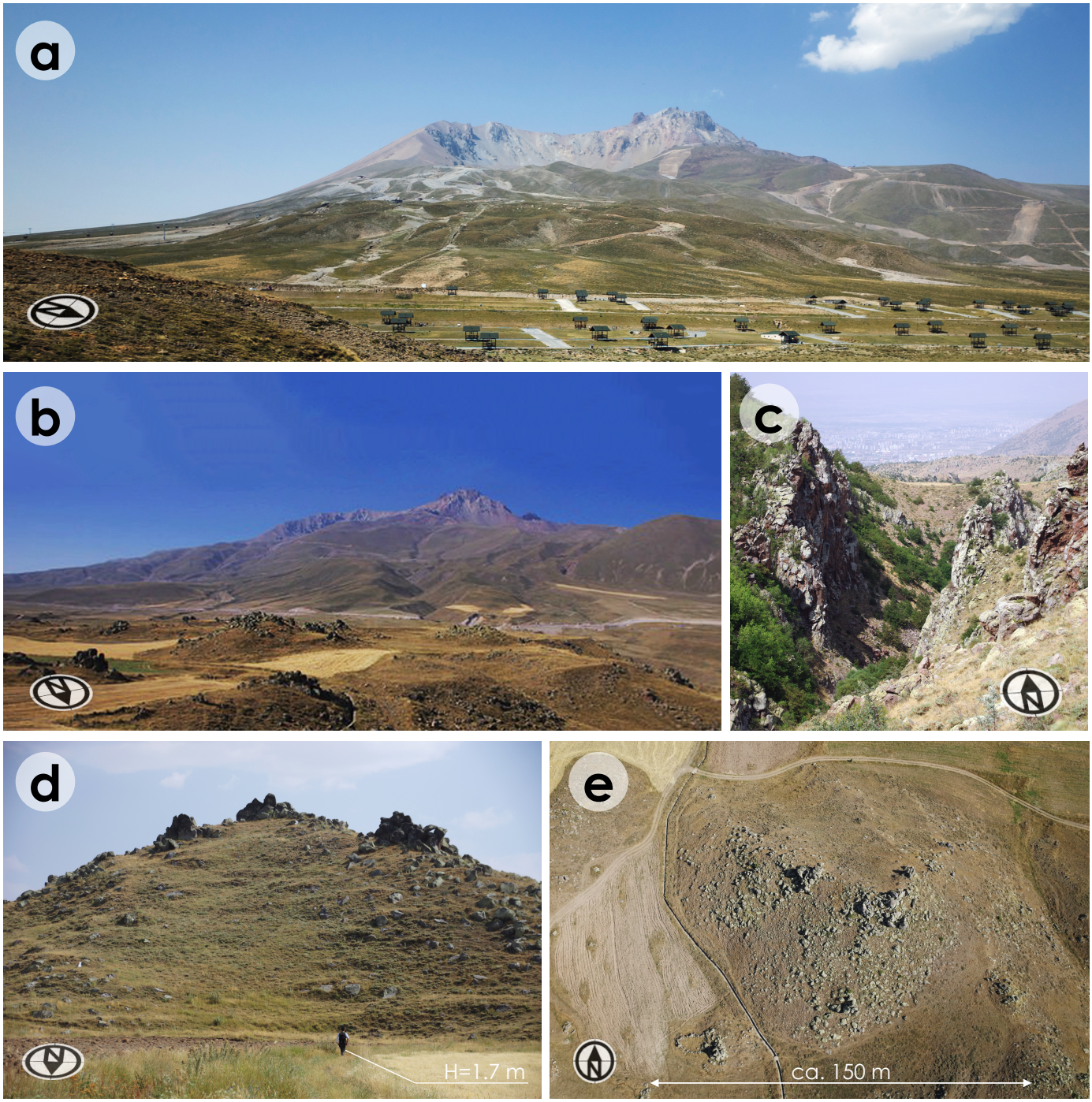

Hayakawa et al. Figure 2.

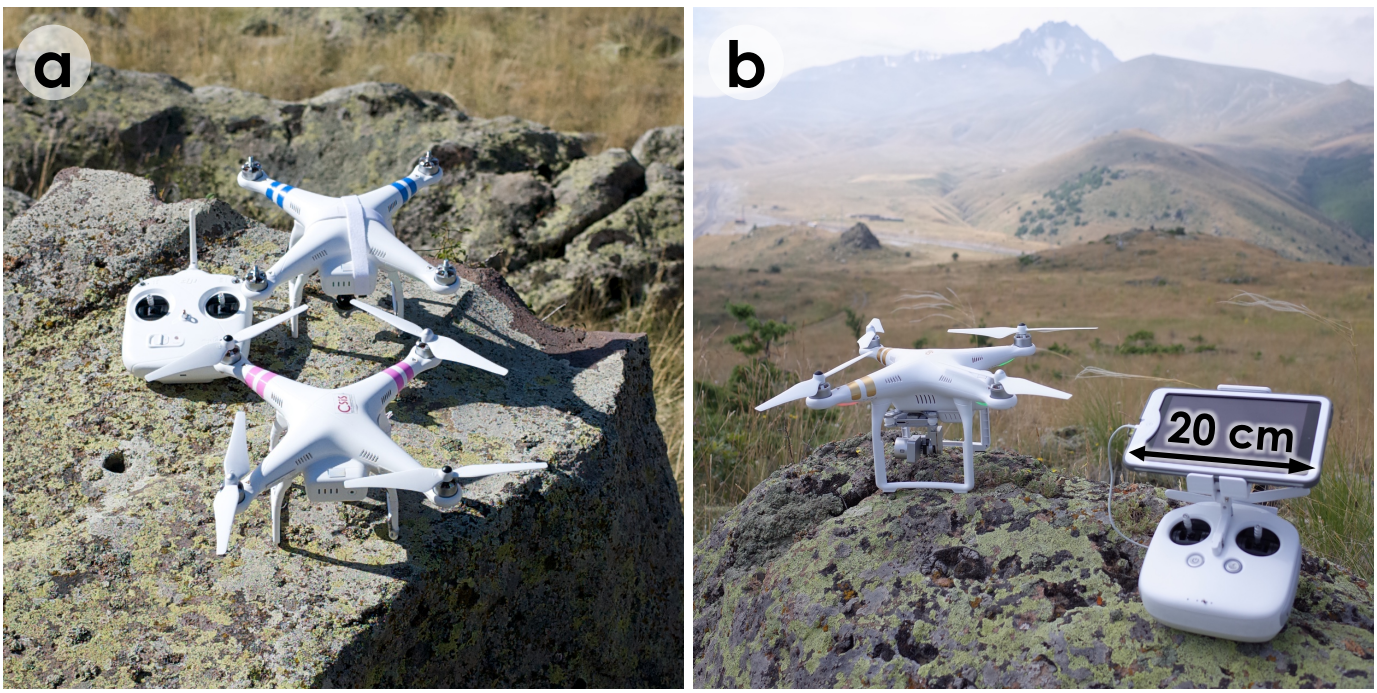

Hayakawa et al. Figure 3.

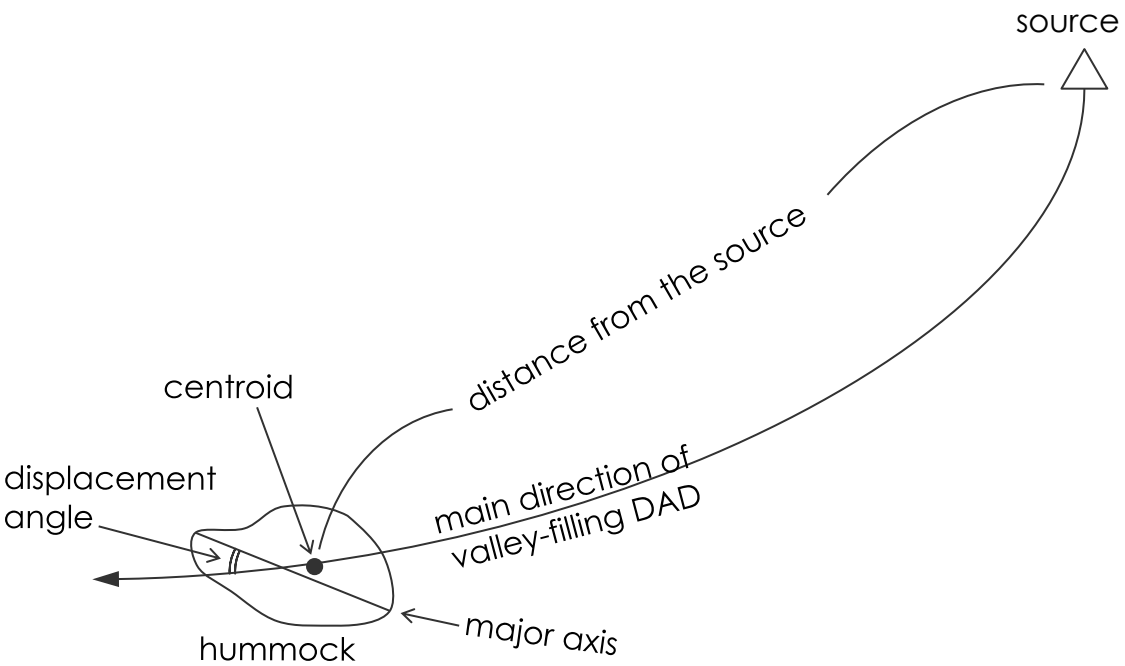

Hayakawa et al. Figure 4.

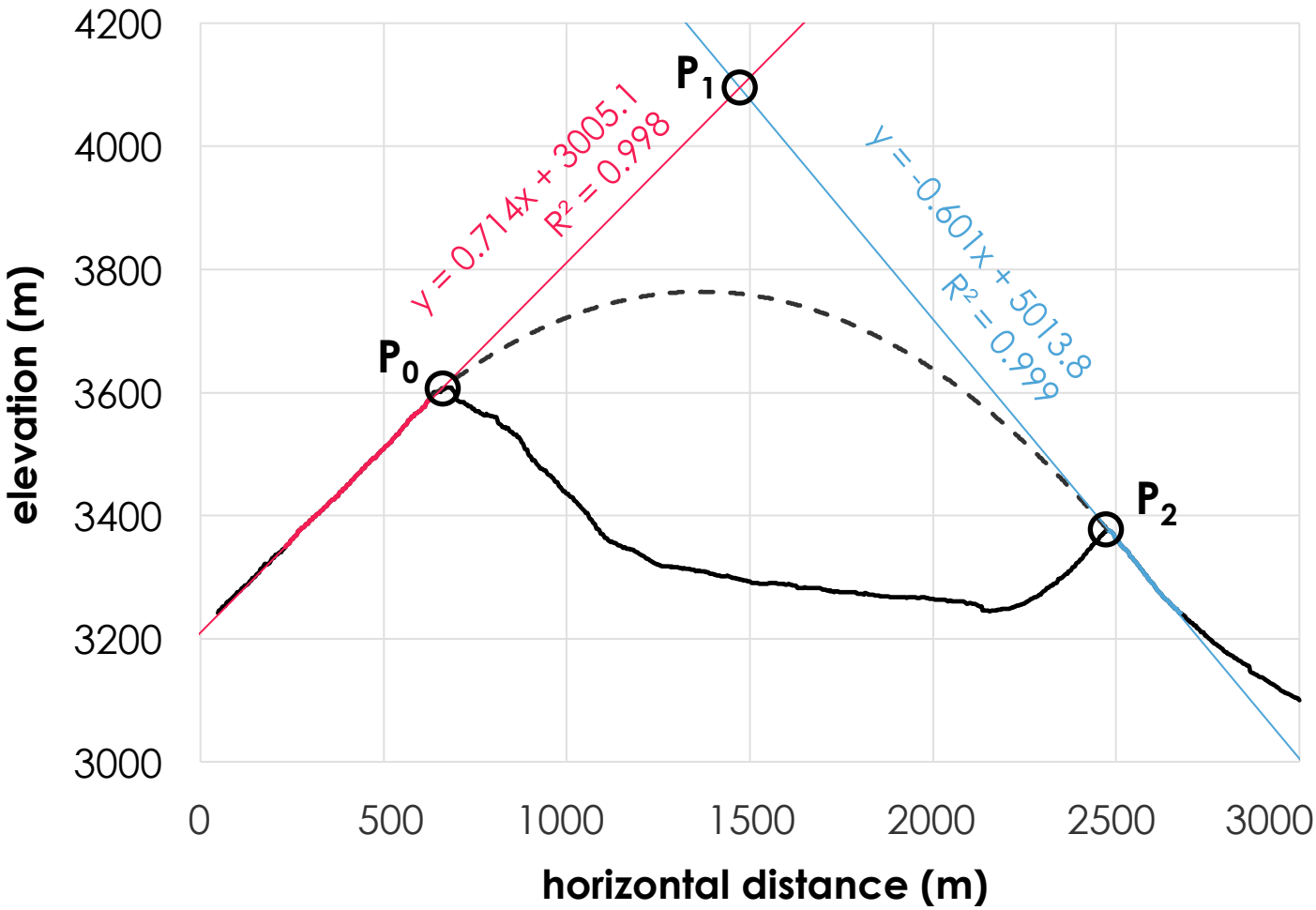

Hayakawa et al. Figure 5.

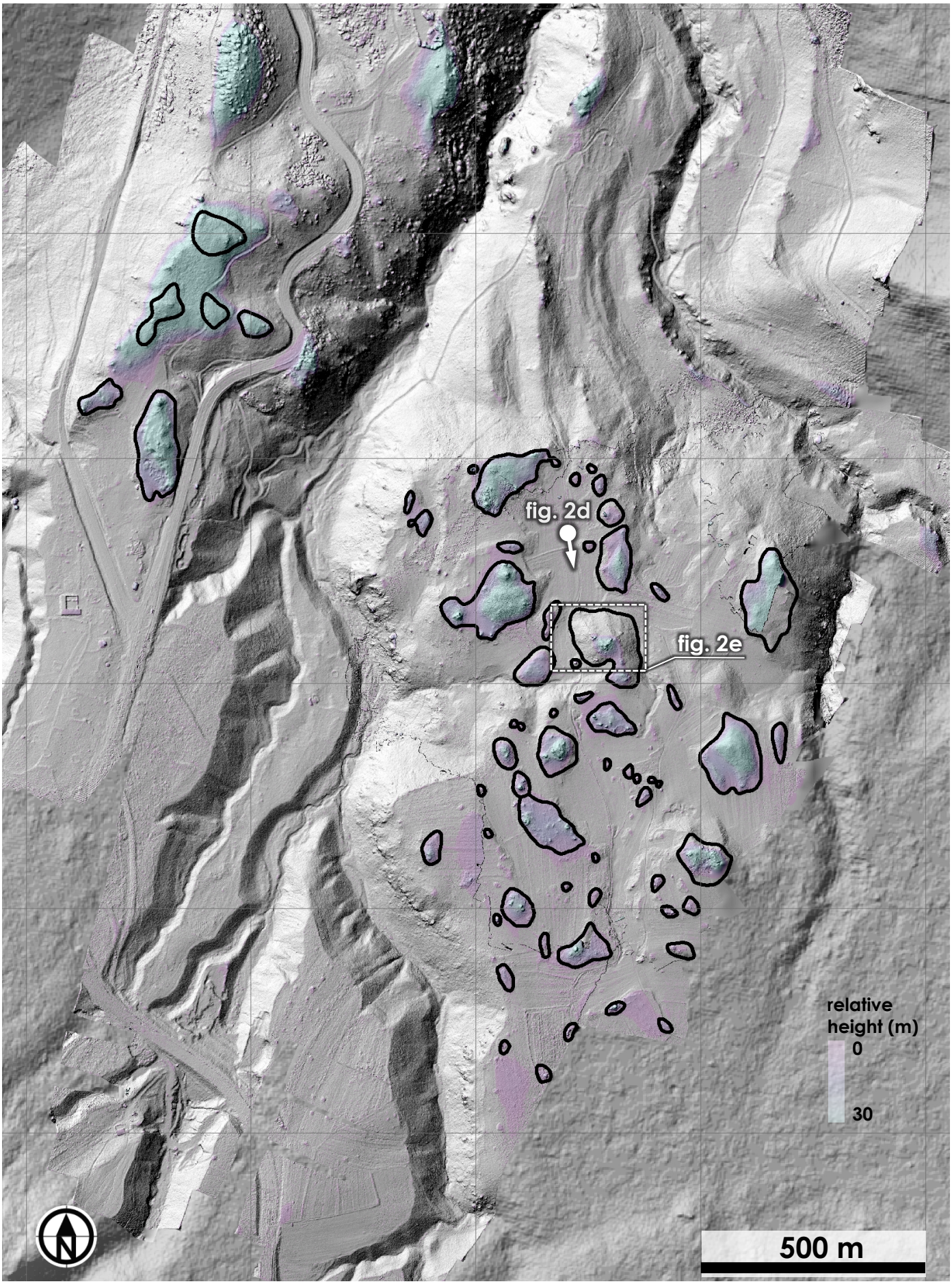

Hayakawa et al. Figure 6.

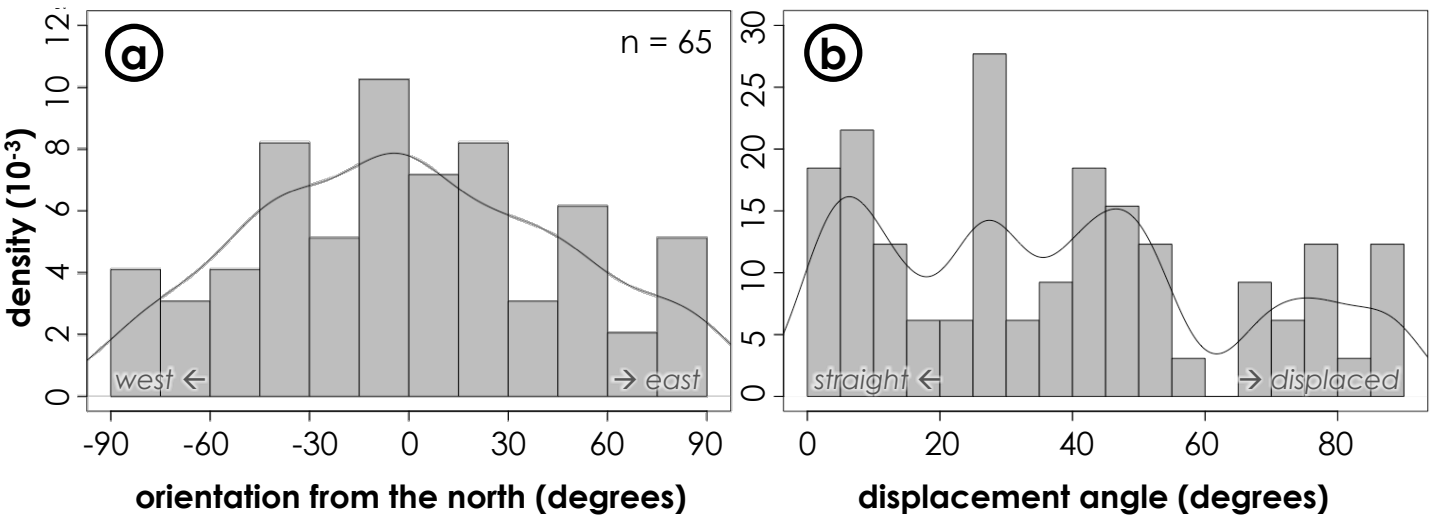

Hayakawa et al. Figure 7.

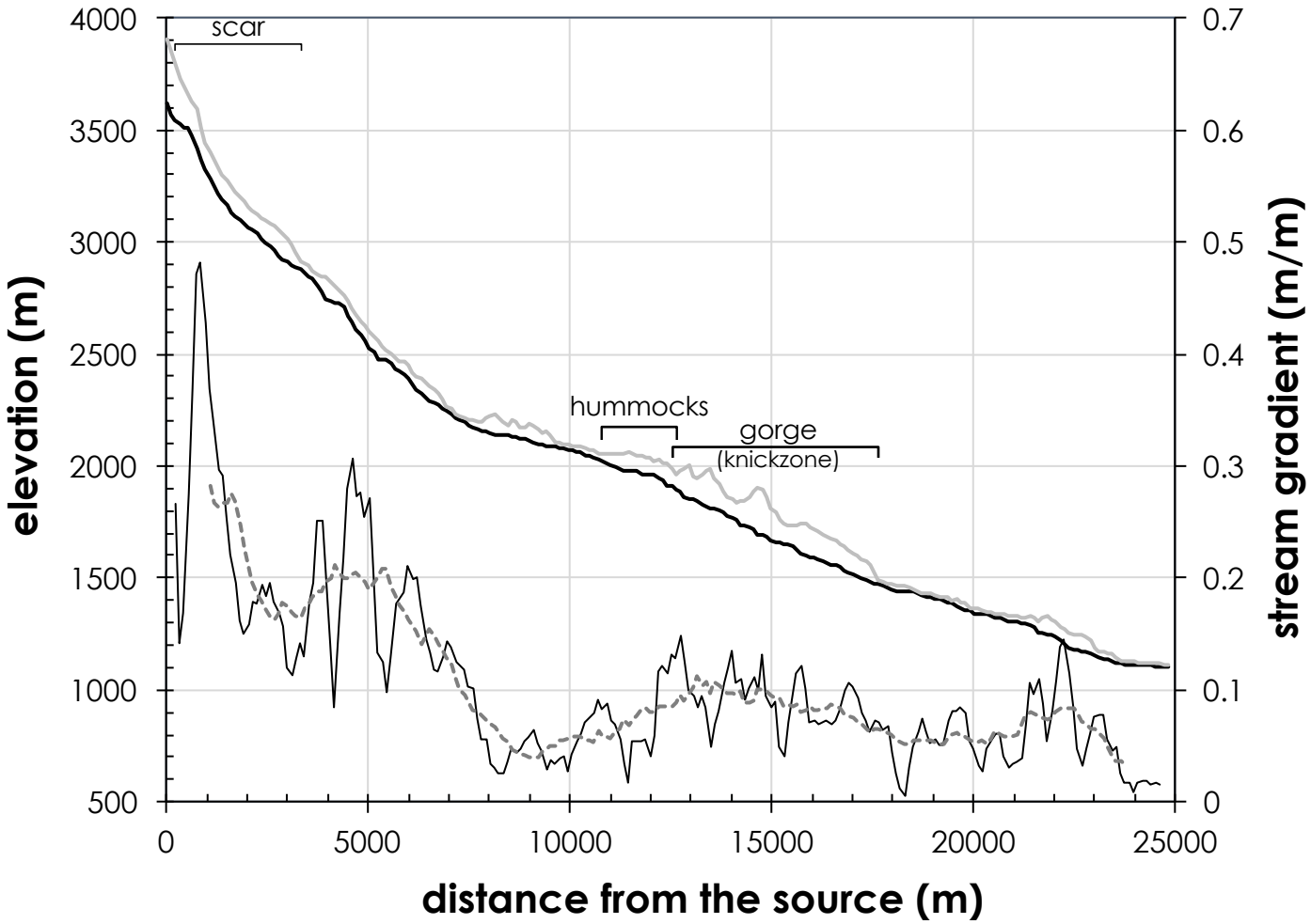

Hayakawa et al. Figure 8.

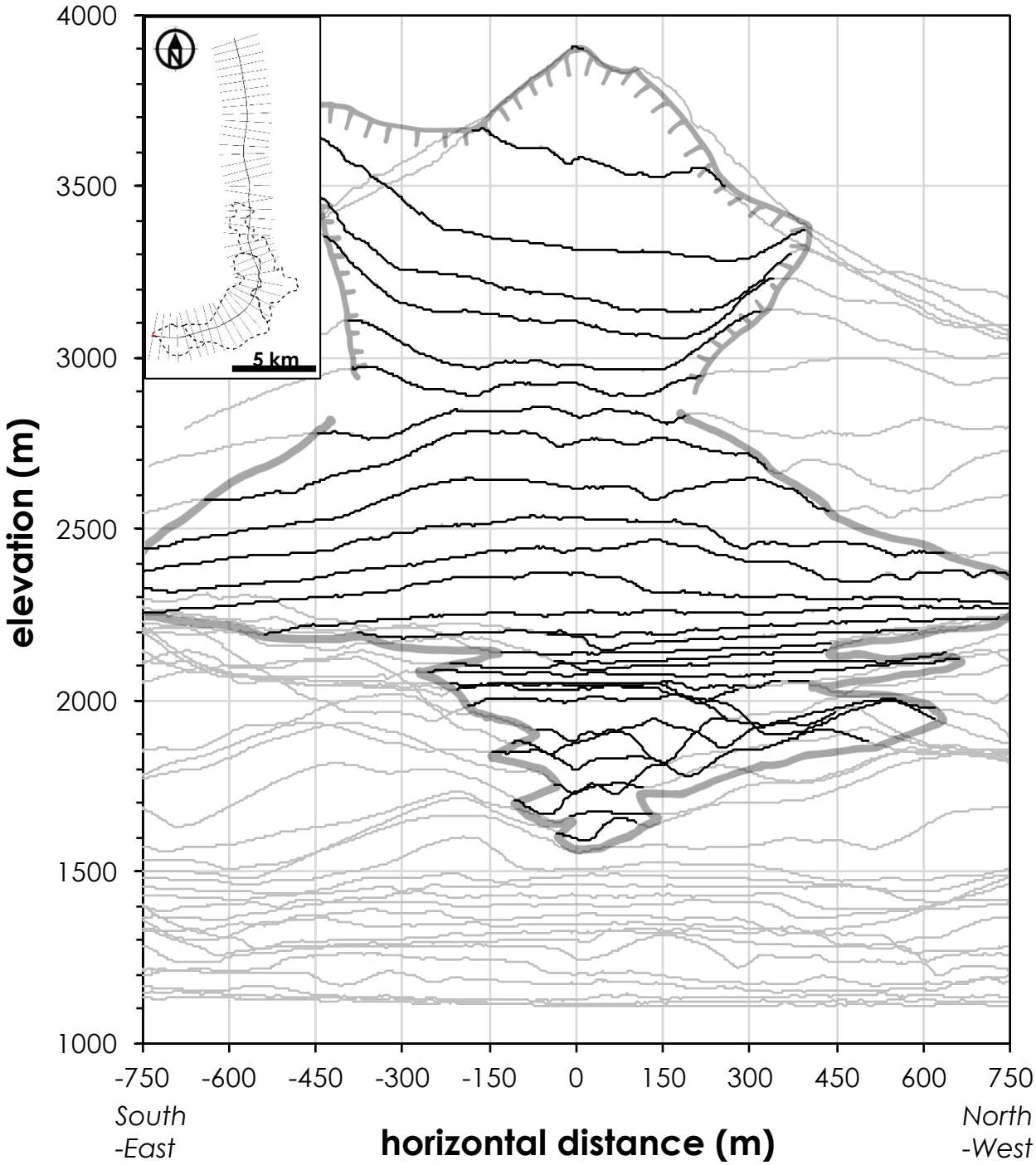

Hayakawa et al. Figure 9.

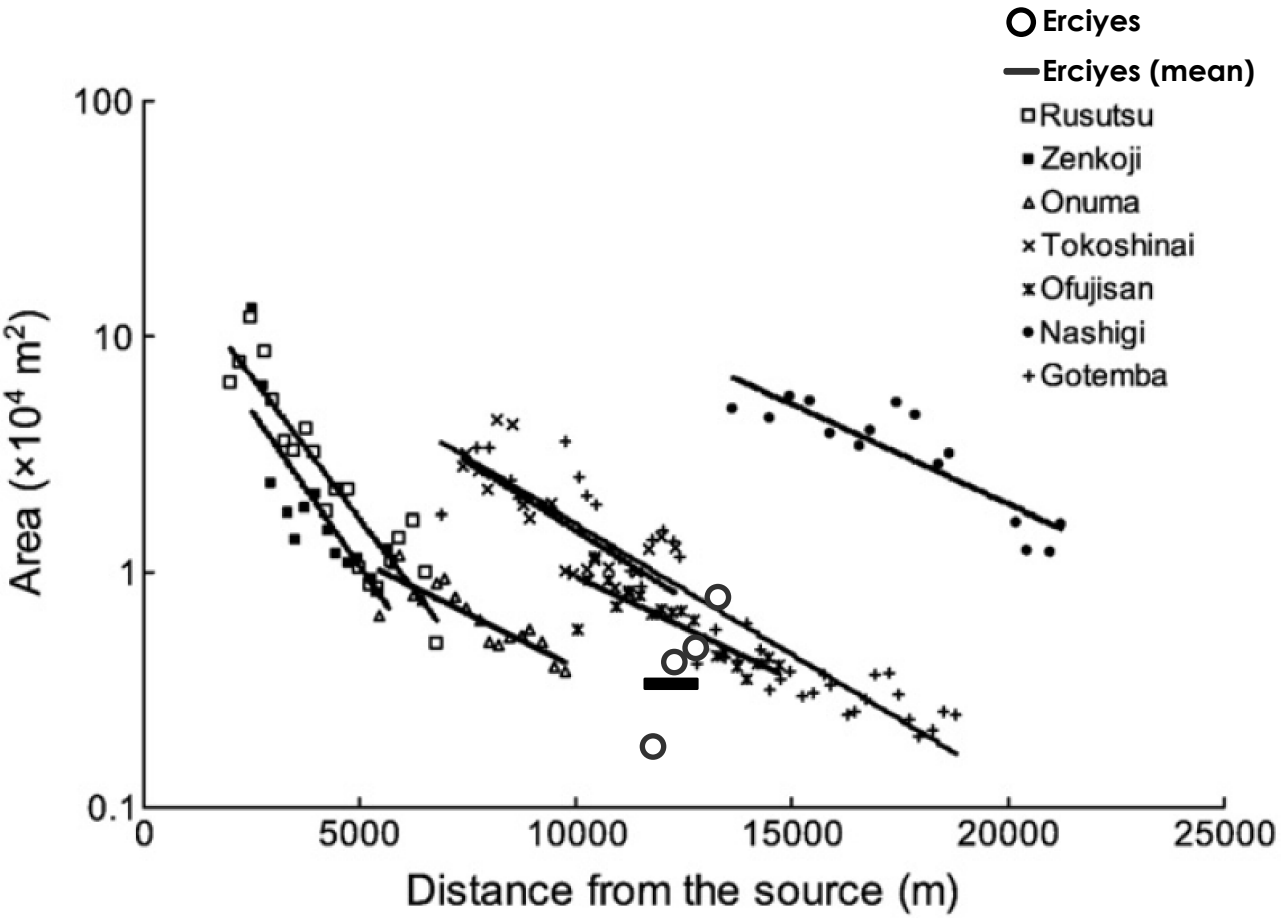

Hayakawa et al. Figure 10.

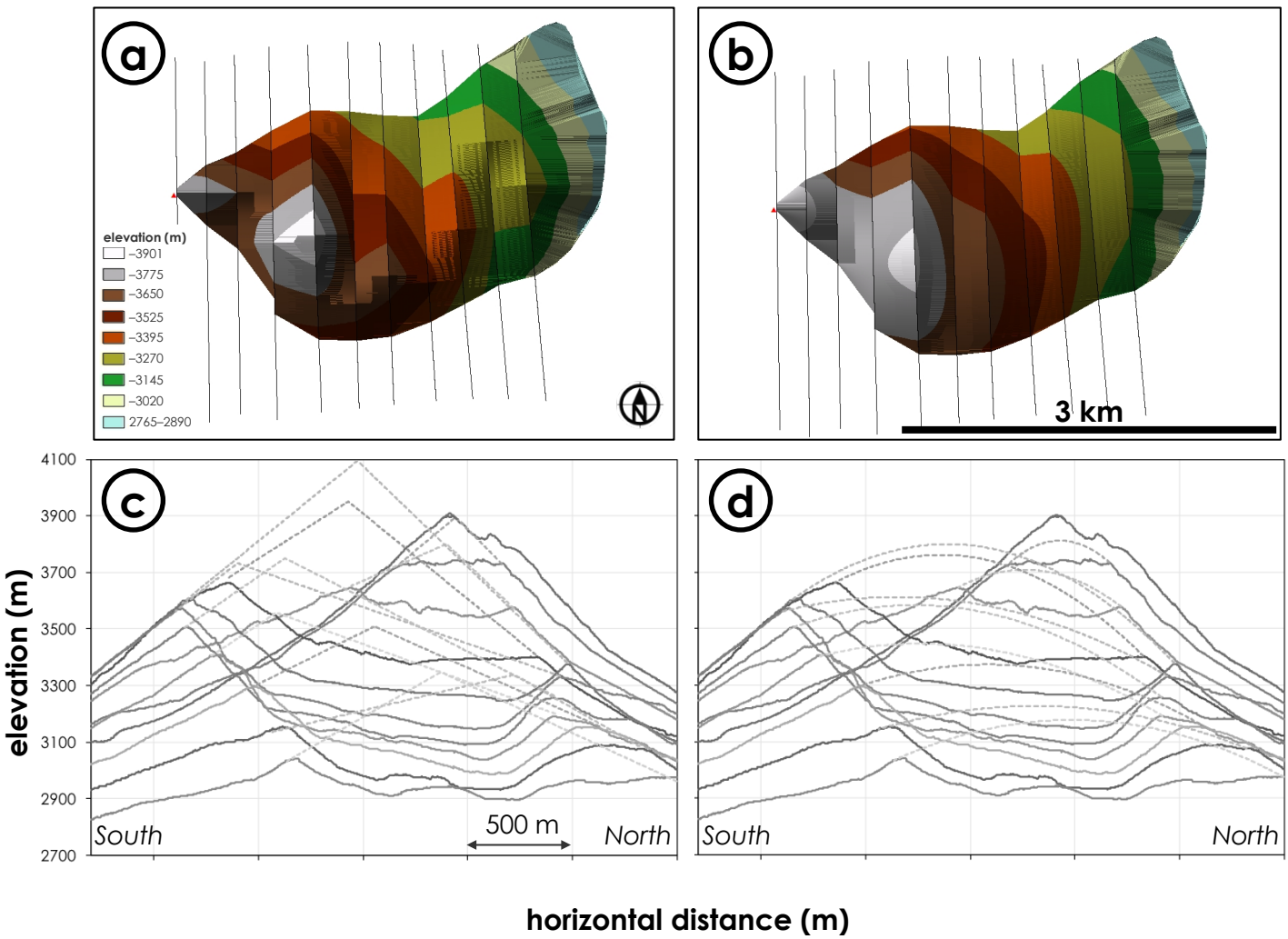

Hayakawa et al. Figure 11.

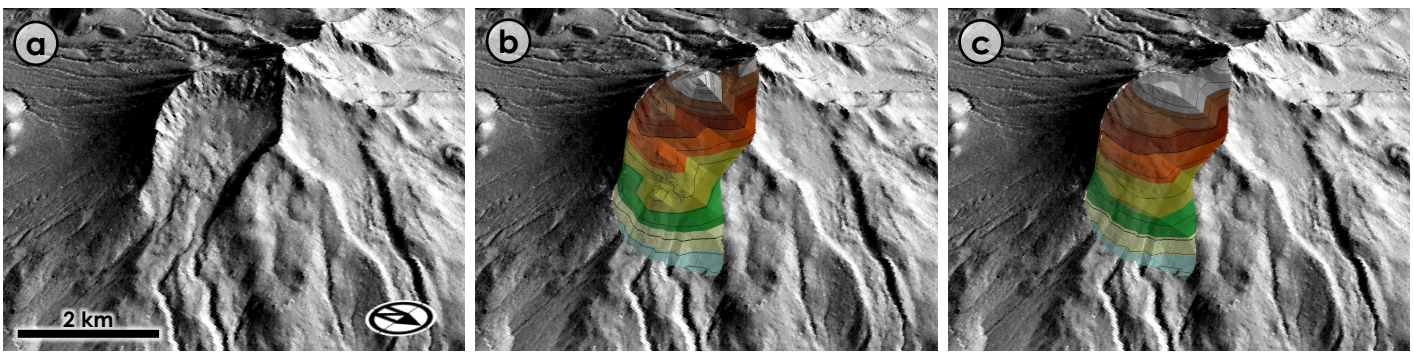

Hayakawa et al. Figure 12.